NIPER/BDM–0174

Topical Report

OIL RECOVERY AND CT-IMAGING OF SURFACTANT-POLYMER CHEMICAL SYSTEMS

by

Bonnie L. Gall, Ph.D. and Feliciano M. Llave, Ph.D.

September 1995

Work Performed Under Contract No.
DE-AC22-94PC91008
Work Authorization 95-A03 Task 2

Prepared for
U.S. Department of Energy
Bartlesville Project Office

NIPER/BDM–0174
Distribution Categories UC-122 and 125
September 1995

Topical Report

OIL RECOVERY AND CT-IMAGING OF SURFACTANT-POLYMER CHEMICAL SYSTEMS

by

Bonnie L. Gall, Ph.D. and Feliciano M. Llave, Ph.D.

Work Performed Under Contract No.
DE-AC22-94PC91008
Work Authorization 95-A03 Task 2

Prepared for
U.S. Department of Energy
Bartlesville Project Office

DISCLAIMER

This report was prepared as an account of work sponsored by an agency of the United States Government. Neither the United States Government nor any agency thereof, nor any of their employees, makes any warranty, expressed or implied, or assumes any legal liability or responsibility for the accuracy, completeness, or usefulness of any information, apparatus, product, or process disclosed, or represents that its use would not infringe privately owned rights. Reference herein to any specific commercial product, process, or service by trade name, trademark, manufacturer, or otherwise does not necessarily constitute or imply its endorsement, recommendation, or favoring by the United States Government or any agency thereof. The views and opinions of authors expressed herein do not necessarily state or reflect those of the United States Government or any agency thereof.

BDM-Oklahoma, Inc.
P.O. Box 2565
Bartlesville, Oklahoma 74005

ABSTRACT

Evaluation of surfactant/polymer Improved Oil Recovery (IOR) systems at NIPER has emphasized the use of mixed surfactant systems to provide design flexibility for different reservoir temperature and salinity conditions. During FY 95, oil recovery screening studies were conducted on a select surfactant system, containing a nonionic and an anionic component. The effects of different variables on the oil recovery potential were evaluated using conventional and CT-monitored coreflood experiments. The parameters evaluated included: chemical injection strategy, chemical slug size, effective permeability, and polymer concentration for mobility control.

Oil recovery was higher for a preequilibrated chemical/oil slug (middle-phase injection) than for injection of the mixed surfactant chemical slug throughout the permeability range tested (100-1,000 mD). Oil recovery was higher for the more permeable cores. For both injection strategies, oil recovery was severely restricted by the poor sweep for the low permeability cores. CT-monitored experiments indicated the presence of relatively high oil saturation "streaks" in the low permeability cores ($\approx$ 100 md) at the end of the chemical flood. Optimal slug size for the system was approximately 25% PV. Higher recoveries were possible using larger chemical slug sizes, but cost also increased significantly.

Polymer loading was studied to determine the effect of improved mobility control on recovery efficiency, particularly for the case of a nonequilibrated chemical slug. Favorable response to the higher polymer loading was observed. High polymer concentrations, however, would be uneconomical for field applications. Oil recovery results were compared with salinity gradient experiments using 1,000 ppm biopolymer for mobility control. The final oil saturations for the salinity gradient experiments were much lower than those obtained using nonequilibrated chemical slugs unless high polymer loadings were used. The salinity gradient approach assures optimal conditions for oil solubilization and mobilization during chemical injection as well as helping to reduce surfactant loss by adsorption and trapping. The overall results support the trend as follows:

500 ppm $\leq$ 1,000 ppm < 1,500 ppm < 2,000 ppm < salinity gradient @ 1,000 ppm < 3,000 ppm

CT imaging to determine oil saturation distributions during a chemical IOR oil recovery experiment was conducted on a characterized Berea sandstone core. The chemical system selected for study has been studied extensively. UTCHEM simulation did not show the buildup of oil saturation in the oil bank that was observed using the CT. The ability to observe and quantify the oil recovery mechanisms using CT imaging improves the evaluation and design of chemical flooding formulations.

ACKNOWLEDGMENT

This work was sponsored by the U. S. Department of Energy under M&O contract agreement DE-AC22-94PC91008. The authors wish to thank Drs. Arfon Jones and Rebecca Bryant of BDM-Oklahoma, Inc. for their guidance and advice in conducting the study. Appreciation is also expressed to Kathleen Bertus, Idell Cook, and Alan Miller also of BDM-Oklahoma for their assistance in all phases of the experimental work, and Dr. Hong Gao and Dr. Liviu Tomutsa for their assistance in simulation studies. The authors also wish to acknowledge Dr. Liviu Tomutsa and Sam Swan of the CT Imaging Group for their expertise, advice, and assistance while conducting the CT-monitored experiments.

TABLE OF CONTENTS

1.0 INTRODUCTION **1**

2.0 EXPERIMENTAL PROCEDURES **3**

2.1 Phase Behavior 3

2.2 Salinity and Alkane Scans 3

2.3 Phase Inversion Temperature (PIT) Measurements 3

2.4 Interfacial Tension (IFT) Measurements 3

2.5 Coreflooding Experiments 4

2.6 Computer-Aided Tomography Imaging Techniques 4

2.7 Mini-permeameter Measurements 4

2.8 Simulation Studies 5

3.0 RESULTS **7**

3.1 Screening of Mixed Surfactant Systems 7

3.2 Oil Recovery Studies Using a Mixed Surfactant System 7

3.2.1 Chemical Injection Strategy 9

3.2.2 Chemical Slug Size 9

3.2.3 Chemical Screening Tests 12

3.2.4 Polymer Concentration 13

3.2.5 CT-Imaging of Mixed Surfactant Coreflood Experiments 18

3.3 CT-Imaging and Simulation Studies of a Surfactant/Polymer IOR System 26

3.3.1 Description of Experiment 26

3.3.2 Core Characterization 28

3.3.3 Description of the Chemical System 34

3.3.4 Oil Recovery and Analysis of Effluents 36

3.3.5 CT-Imaging and Simulation of Tracer 39

3.3.6 CT-Imaging and Simulation of Chemical Flood 44

4.0 SUMMARY AND CONCLUSIONS **51**

5.0 REFERENCES **53**

APPENDIX A **55**

APPENDIX B **59**

TABLES

3–1 Description of Experiments for Mixed Surfactant Oil Recovery Experiments 10
3–2 Core Properties and Permeabilities for CT-CF 12 27
3–3 Fluid Compositions Used During CT-CF 12 Chemical Flood Experiment 27
3–4 Fluid Injection and CT Imaging Sequence for CT-CF 12. 28
3–5 Summary of Initial Fluid Volumes and Fluid Volumes After Injection of 0.52 PV Surfactant and Polymer Slugs 48
A–1 NIPER Coreflood Report—CT-CF 12. 56
B–1 Input Parameters for Simulation of a Surfactant/Polymer Coreflood Using UTCHEM 59

FIGURES

3–1 Measured IFT Values Versus Salinity Using Hepler Oil. 8
3–2 Measured IFT Values Versus Time Using Hepler Oil. 8
3–3 Comparison of Oil Saturation (S_{ocf}) vs. Brine Permeability. 11
3–4 Comparison of Oil Saturation (S_{ocf}) vs. Chemical Slug Size. 11
3–5 Phase Inversion Temperature (PIT) for 1.0 wt% DM-530 + 1.0 wt% Petronate L/IBA with n-Heptane and 500 ppm Polymer. 13
3–6 Phase Inversion Temperature (PIT) for 1.0 wt% DM-530 + 1.0 wt% Petronate L/IBA with n-Heptane and 1,000 ppm Polymer. 14
3–7 Phase Inversion Temperature (PIT) for 1.0 wt% DM-530 + 1.0 wt% Petronate L/IBA [1:1] with n-Heptane. 14
3–8 Effect of Polymer Loading on Phase Behavior of DM-530 + Petronate L/IBA System with n-Heptane. 15
3–9 Residual Oil Saturation vs. Polymer Concentration. 15
3–10 Oil Cut vs. Pore Volume Injected Using Different Polymer Concentrations. 16
3–11 Oil Recovery vs. Pore Volume Injected Using Different Polymer Concentrations. 17
3–12 CT-monitored Flow Profile for Experiment 23 (L to R). 19
3–13 CT-monitored Flow Profile for Experiment 24 (L to R). 21
3–14 CT-monitored Flow Profile for Experiment 42 Using 1,500 ppm Polymer. 22
3–15 CT-monitored Flow Profile for Experiment 44 Using 2,000 ppm Polymer. 23
3–16 CT-monitored Flow Profile for Experiment 48 Using 3,000 ppm Polymer. 24
3–17 Schematic of Core for Simulation of CT-monitored Chemical Oilflood Experiment, CT-CF 12. 29
3–18 Minipermeameter Permeability Measurements of the End Faces (Sides 5 and 6) of Core CT-CF 12. 29
3–19 Minipermeameter Permeability Measurements of Sides 1 and 2 of Core CT-CF 12. 30
3–20 Minipermeameter Permeability Measurements of Sides 3 and 4 of Core CT-CF 12. 31
3–21 Permeability/Porosity Correlation for Berea Sandstone Core from Minipermeameter and PIA Analysis. 32
3–22 Porosity Map for CT-CF 12. 33
3–23 Average Porosity for CT-CF 12 from Side 6 to Side 5. 33
3–24 Profile of Brine Tracer Through Core CT-CF 12 for Various Amounts of Injected Fluid. 34
3–25 Phase Volume Fraction Diagram for Petroleum Sulfonate/Alcohol/Decane/ Brine System as a Function of Brine Salinity. 35
3–26 Viscosity as a Function of Shear Rate for 1,000 ppm Xanthan Biopolymer. 36
3–27 Cumulative Oil Production and Oil Cut for CT-CF 12. 37
3–28 Pressure History and Production of Surfactant and Polymer During CT-CF 12. 38

3–29 Comparison of Surfactant Production Curves for CT-CF 12 and for Camilleri's Results (1987a, see Figs. 8 and 9). 39
3–30 Average Tracer Profile After 0.46 PV Injected for a Simulation Using UTCHEM as Compared With the Average Tracer CT Image Profile. 40
3–31 Simulated Profile of Brine Tracer Through Core CT-CF 12 for Various Amounts of Injected Fluid Using a 35 x 63 Permeability/Porosity Grid with PC-GEL. 40
3–32 Simulated Profile of Brine Tracer Through Core CT-CF 12 Using a 10 x 62 Permeability/Porosity Grid with PC-GEL. 41
3–33 Density of Sodium Iodide in 3 wt% Potassium Chloride. 42
3–34 Simulation of CT-CF 12 Tracer Using BOAST. 42
3–35 Comparison of the Tracer Fluid Fronts from CT Data and Simulations for 0.20 PV Fluid Injected. 43
3–36 Comparison of the Tracer Fluid Fronts from CT Data and Simulations for 0.20 PV Fluid Injected. 43
3–37 Comparison of the Tracer Fluid Front from CT Data and Simulations for 0.82 PV Fluid Injected. 44
3–38 CT Images of Oil Saturation Distributions After Oil Flood and Waterflood for CT-CF 12. 45
3–39 Average Oil Saturation Along the Core After Oil Flood and for Test CT-CF 12 Waterflood. 45
3–40 Oil Saturation Distribution During CT-CF 12 Chemical Flood. 46
3–41 Comparison of the Oil Saturation Distribution After Surfactant Slug Injection of a Single Slice (1), One Pixel Wide, Down the Middle of the Core With the Average Oil Saturation for 140 Pixels (2). 47
3–42 Comparison of the CT oil Saturation Distribution After Injection of 0.52 PV With the Simulated Oil Saturation Distribution Shown in Figure 11 of Camilleri's Paper. 48

1.0 INTRODUCTION

Evaluation of surfactant/polymer Improved Oil Recovery (IOR) systems at NIPER has emphasized the use of mixed surfactant systems to improve performance for higher salinity and temperature conditions. Chemical flooding has the capability of recovering more residual crude oil than most other available IOR methods. However, sensitivity to changes in reservoir conditions, loss of effectiveness caused by chemical depletion, dilution, and separation, and cost have limited the application of chemical IOR. Mixed surfactant systems are adaptable to different reservoir conditions of salinity, temperature, and oil type and can be designed to achieve improved tolerance, when compared to single component surfactant systems. Equally important are processes to sustain the movement of oil, mobilized by effective chemical systems, to the production well. Failure to maintain effective mobility control has been identified as an important problem in both laboratory and field applications of chemical flooding systems.

For many U. S. domestic oil reservoirs, chemical flooding may be the only viable means of extending their productive lives. Broad based studies, including evaluating different chemical systems and optimizing application parameters, must be conducted for efficient and economic application at current and projected oil prices.

Previous studies at NIPER have included screening of mixed surfactant systems to determine conditions where the chemical systems produce the most favorable phase behavior, oil solubilization, and low interfacial tension properties (Llave et a. 1990, 1992a, 1992b, 1993, 1994). Computer-aided tomography (CT) imaging techniques were utilized to visualize oil movement and to separate the effects of core properties from those of the chemical formulation (Gall, 1992). During FY 1995, laboratory studies have concentrated on examining the effects of mixed surfactant injection strategy, chemical slug size, core effective permeability and polymer concentration for mobility control. Both conventional and CT-monitored corefloods were conducted. Efforts were also made to simulate the oil saturation distributions during various stages of an oil recovery experiment using a chemical flooding simulator, UTCHEM. This report describes the results of these coreflooding experiments for the DOE sponsored research project Chemical-Including Formation Stimulation - Improved Recovery Processes (A03-Task 02).

2.0 EXPERIMENTAL PROCEDURES

2.1 Phase Behavior

Phase behavior studies were conducted to screen selected mixed surfactant systems for IOR application. These tests were conducted as the basis of the selection process for identifying systems that were used in the oil displacement experiments. These tests included conducting conventional salinity and alkane scans, interfacial tension measurements, phase inversion temperature determination, and compatibility screening. Conditions were defined where 2- and 3-phase regions were observed. Different types of surfactant/brine/oil emulsions are defined as (1) upper phase emulsions with surfactant and some water in the oil phase (type II+), (2) middle phase microemulsion with surfactant in a middle phase with both oil and water (type III), and (3) lower phase emulsions with surfactant and some oil in the water phase (type II-).

2.2 Salinity and Alkane Scans

Conventional salinity and alkane scans were conducted on a select system of anionic and nonionic surfactant to determine relative proximity of optimal conditions for coreflooding displacement application. From these studies, optimal salinity and alkane range were determined and used for further evaluation. Solubilization parameters were determined and optimal salinity and alkane combinations were identified. Specific details regarding this test and calculations of solubilization parameters from these scans are discussed in an earlier report (Lorenz and Brock 1987).

2.3 Phase Inversion Temperature (PIT) Measurements

Routine measurement of phase inversion temperature (PIT), in combination with salinity and alkane scans, were used in determine conditions where the selected mixed chemical system could be applied. This method was particularly applicable for the selected nonionic-anionic chemical systems that exhibit dramatic phase transitions with temperature or salinity gradients. The PIT apparatus and the experimental procedures used in the study was discussed extensively in earlier reports measurements were conducted using a computer-controlled apparatus designed and constructed at NIPER (Llave and Olsen 1988).

2.4 Interfacial Tension (IFT) Measurements

The interfacial tensions (IFT) of the different chemical systems were measured using a Model 300 Spinning Drop Interfacial Tensiometer, manufactured at University of Texas at Austin. These

measurements were conducted using different equilibrated chemical systems at selected temperature conditions. These measurements were taken after sufficient time was allowed for equilibration at the test temperature. Measurements were performed until reproducible values were obtained. Fluid densities were measured using a Mettler/Paar DMA 45 Calculating Digital Density Meter; and refractive indices were measured using a Bausch & Lomb Refractometer. Details of these experimental and calculation procedures were reported previously (Llave et al. 1990).

2.5 Coreflooding Experiments

Coreflooding experiments were conducted with several chemical systems. A series of these experiments evaluated the effect of injection strategy, slug size, chemical slug formulation, permeability, and mobility control on overall oil displacement capacity. The experiments were conducted using Berea sandstone core plugs (3.8 cm in diameter and about 24 cm in length) of different brine permeabilities. Experimental procedures for core saturation, porosity and permeability measurement, and chemical injection were described in earlier reports (Llave et al. 1992). The injection strategy (oil displacement strategy) employed was systematically varied and designed to identify effects of different parameters on the overall displacement efficiency. Some of these experiments were monitored with the NIPER's CT-imaging capability.

2.6 Computer-Aided Tomography Imaging Techniques

CT equipment, operating procedures, and image processing techniques at NIPER have been described previously (Tomutsa et al. 1990; and Gall, 1992). Oil saturation distributions within the core were determined at various stages of a chemical core flooding experiment. The formation and shape of the oil bank can be observed during surfactant injection, as well as the efficiency of the chemical slug to produce oil from the core. The influence of core heterogeneities on oil mobilization can also be observed.

2.7 Mini-permeameter Measurements

A mini-permeameter was constructed to allow rapid determination of permeability distribution. The apparatus measures gas flow and pressure drop at the interface of a small tube pressed against the rock surface. The instrument is calibrated using rock samples of known permeability. An automated table allows multiple measurements for predetermined grid patterns with minimum effort.

2.8 Simulation Studies

Three simulators were used to predict tracer movement through the core samples. They included BOAST-VHS, a black oil simulator modified at NIPER (Chang et al. 1991), PC-GEL, a simulator developed at NIPER to determine the effectiveness of profile modification treatments on oil production (Gao and Chang, 1990), and UTCHEM, a chemical flooding simulator developed and modified at the University of Texas (Pope and Nelson, 1978). The present version, UTCHEM V-5.31, was available for the study.

3.0 RESULTS

3.1 Screening of Mixed Surfactant Systems

Phase behavior studies were conducted on a select surfactant system. The system tested was formulated with a commercially available petroleum sulfonate surfactant (Witco™ Petronate L) and isobutyl alcohol (IBA) [5:3] in 1% NaCl. The Petronate L sample was recommended by the manufacturer as a suitable replacement for the traditional Witco™ TRS 10-410 (Private communication).

An alkane scan was conducted using Petronate L at ambient temperature to compare with previous alkane scans using TRS. The scan with n-decane appeared to exhibit optimal behavior for this system (optimal solubilization parameter $\approx$ 14.5 mL/mL). A surfactant mixture of Petronate L/IBA and Igepal™ DM-530 surfactants [1:1] was also evaluated. The overall results were similar to the behavior exhibited by the TRS 10-410 surfactant.

Other chemical systems were also screened. The preliminary screening included interfacial tension measurements (IFT) on two chemical systems containing low concentration surfactants samples with alkaline additives. These mixtures contained 0.5 wt% surfactant (experimental petroleum sulfonates, EOR 1989 and EOR 1988) with 0.095N $NaHCO_3$ and 0.095N Na_2CO_3. IFT vs. salinity scans (0.0% NaCl to 3.0% NaCl) were conducted with these formulations.

Figure 3–1 shows the results of the IFT measurements as a function of salinity (wt% NaCl up to 3.0%) conducted using Hepler field crude oil (Crawford County, KS). The results showed very favorable interfacial activity for a very limited range of salinity values. Fairly low IFT values, within the 10^{-3} mN/m range, were measured for salinities around 0.5 to 1.0 wt% NaCl. Figure 3–2 shows the plot of the IFT measured versus time at the different salinities tested. One favorable aspect of the IFT behavior was that these systems initially generated relatively low IFT values and remained low throughout the test.

The level of alkaline additive used in these tests was arbitrary and not optimized for improved interfacial activity. Additional screening work under Task 1, "Alkaline Flooding" was conducted to further evaluate the potential of this mixed system.

3.2 Oil Recovery Studies Using a Mixed Surfactant System

The effect of different variables on the oil recovery potential of a select chemical system, containing a nonionic and an anionic component, was evaluated. The chemical system used was Petronate-L/IBA + DM-530 [1:1]. Results from these experiments tie-in directly with the phase behavior results presented in an earlier NIPER/BDM report (Llave et al. 1994).

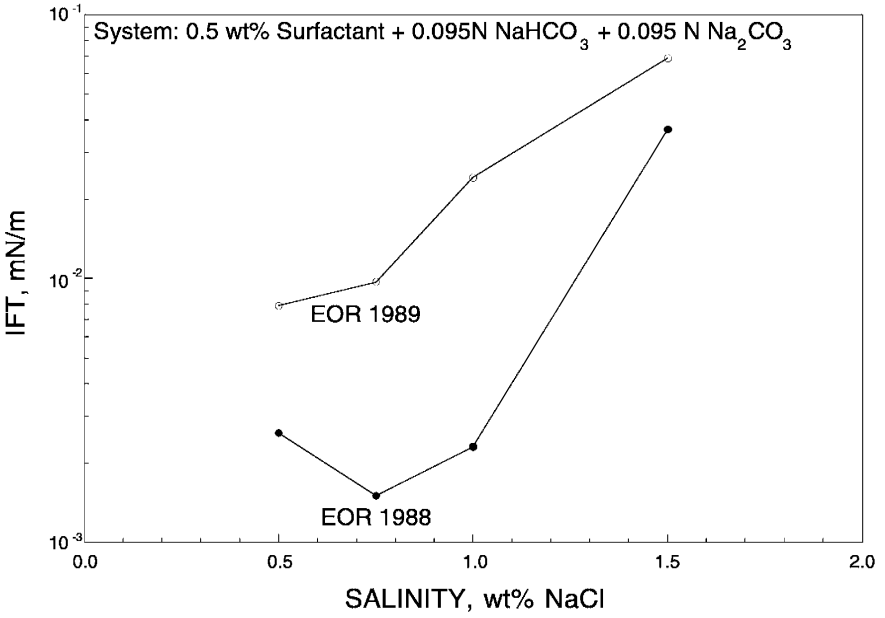

Figure 3–1 Measured IFT Values Versus Salinity Using Hepler Oil.

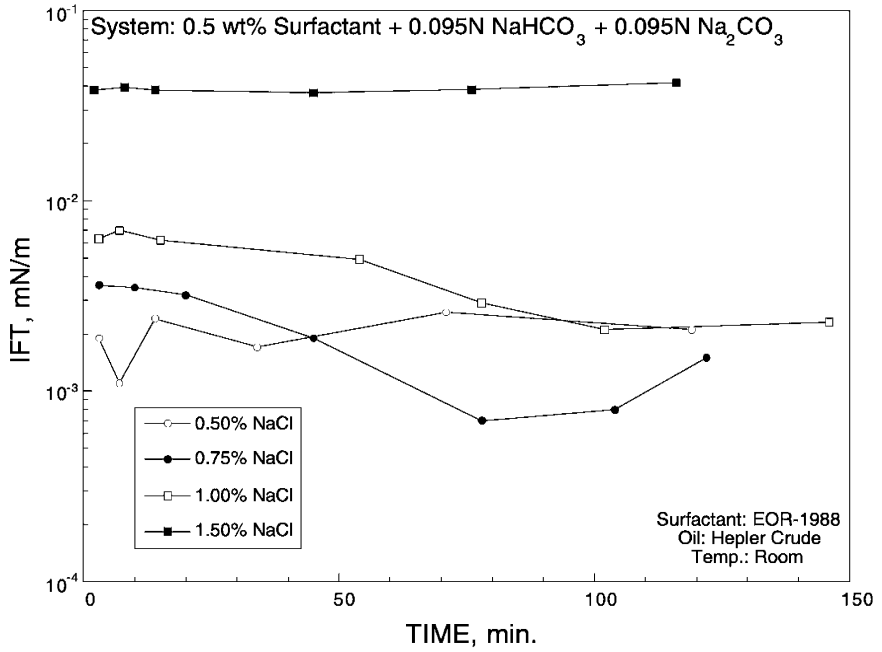

Figure 3–2 Measured IFT Values Versus Time Using Hepler Oil.

The experimental conditions, pertaining to the selection of the alkane, salinity conditions, and experimental parameters, are based on the results of the earlier reported phase behavior studies. For experimental convenience, a system was selected for further study that exhibited optimal phase behavior at room temperature. Favorable phase behavior and low IFT's were measured at ambient temperature for the mixed surfactant system in 2.5% NaCl brine with n-heptane. CT-monitored experiments required the use of a tagging agent in the oil phase (iododecane). Addition of iododecane to n-heptane did not shift optimal phase behavior conditions. A systematic oil recovery study determined the effect of several variables including: injection strategy, slug size, chemical slug formulation, permeability, polymer concentration, and mobility control. The results of the study are presented in Figures 3-3 through 3-16. A detailed listing of the experiments conducted and the results are summarized in Table 3–1. Experiment nos. 1 to 22 were described in an earlier report (Llave et al. 1994).

3.2.1 Chemical Injection Strategy

As mentioned earlier, conventional coreflooding experiments and CT-monitored experiments were conducted. Cores of different effective permeability were used in these experiments. The oil displacement potential of the straight chemical system (injected as a slug) was evaluated and compared to the results using the middle-phase slug. The oil displacement efficiency in these experiments was compared at initial oil saturation level and at residual oil saturation (after the waterflood). The results favor the high permeability ranges to yield improved oil recovery. The injection of middle-phase chemical slugs yielded better oil displacement compared to the straight (nonequilibrated) chemical injection.

Figure 3–3 shows a plot of the oil saturation vs. brine permeability for the experiments. The effect of brine permeability on achievable oil saturation reduction is evident. The difference in oil recovery for the two injection strategies is also very evident in Figure 3–4. Under the conditions tested, the middle-phase slug yielded lower post-test oil saturation values than the straight slug. The effect of permeability on oil recovery has been observed previously (Llave et al. 1992b). Oil saturation after chemical flood (S_{ocf}) is not as low, however, as that achieved by a large pore volume (PV) alkaline-surfactant-polymer (ASP) slug. A slightly lower total amount of surfactant was used in the ASP formulation. The difference in oil recovery can be attributed differences in phase behavior of the chemical systems and use of a salinity gradient for the ASP injection strategy.

3.2.2 Chemical Slug Size

Optimal chemical slug size tests were conducted for this chemical system using Berea sandstone core samples of relatively high permeability (750 to 950 mD). The target chemical activity for both sets of experiments was 2 wt% active. The middle-phase slugs have a fixed preequilibrated oil content of about 37.5%, yielding a chemical activity of about 1.25 wt%.

Table 3–1 Description of Experiments for Mixed Surfactant Oil Recovery Experiments

Test No.	W.F.*	Perm md	Slug PV %	Oil in Slug, %	Oil in Core	S_{oi} %	S_{owf}^* %	S_{ocf}^* %	R_{eff}^* %OOIP	R_{eff}^* %S_{owf}	Injection Sequence
22	no	842	25.4	0.0	Heptane	66.3	-	27.2	58.9		(no 3-Ø) C.F. + 1,000 P.F. + W.F.
23	no	100	26.0	22.0	80:20	61.8	-	26.8	56.8		3-Ø C.F. + 1,000 P.F. + W.F.
24	no	825	24.3	0.0	80:20	76.0	-	36.5	52.0		(no 3-Ø) C.F. + 1,000 P.F. + W.F.
25	yes	885	27.7	0.0	80:20	75.0	42.6	30.5	59.3	28.4	W.F. + (no 3-Ø) C.F. + 1,000 P.F. + W.F.
26	no	755	25.6	0.0	Heptane	66.6	-	31.4	52.8		(no 3-Ø) C.F. + 1,000 P.F. + W.F.
27	no	532	25.2	0.0	Heptane	70.4	-	31.1	55.8		(no 3-Ø) C.F. + 1,000 P.F. + W.F.
28	no	860	25.1	0.0	Heptane	66.0	-	26.5	59.8		(no 3-Ø) C.F. + 1,000 P.F. + W.F.
29	no	152	25.0	0.0	Heptane	68.2	-	34.4	49.5		(no 3-Ø) C.F. + 1,000 P.F. + W.F.
30	yes	117	25.4	0.0	Heptane	66.7	42.6	37.6	43.4	11.6	W.F. + (no 3-Ø) C.F. + 1,000 P.F. + W.F.
31	yes	444	25.2	0.0	Heptane	68.5	29.5	28.0	59.1	5.3	W.F. + (no 3-Ø) C.F. + 1,000 P.F. + W.F.
32	yes	774	10.0	0.0	Heptane	66.8	40.4	37.7	43.4	6.5	W.F. + (no 3-Ø) C.F. + 1,000 P.F. + W.F.
33	yes	890	25.0	0.0	Heptane	66.3	36.3	28.2	57.5	22.3	W.F. + (no 3-Ø) C.F. + 1,000 P.F. + W.F.
34	yes	883	50.0	0.0	Heptane	68.8	40.2	27.9	59.4	30.7	W.F. + (no 3-Ø) C.F. + 1,000 P.F. + W.F.
35	yes	758	25.0	37.5	Heptane	71.6	40.0	19.6	72.6	51.1	W.F. + C.F. + 1,000 P.F. + W.F.
36	yes	830	9.9	37.5	Heptane	73.8	40.1	36.8	50.1	8.2	W.F. + C.F. + 1,000 P.F. + W.F.

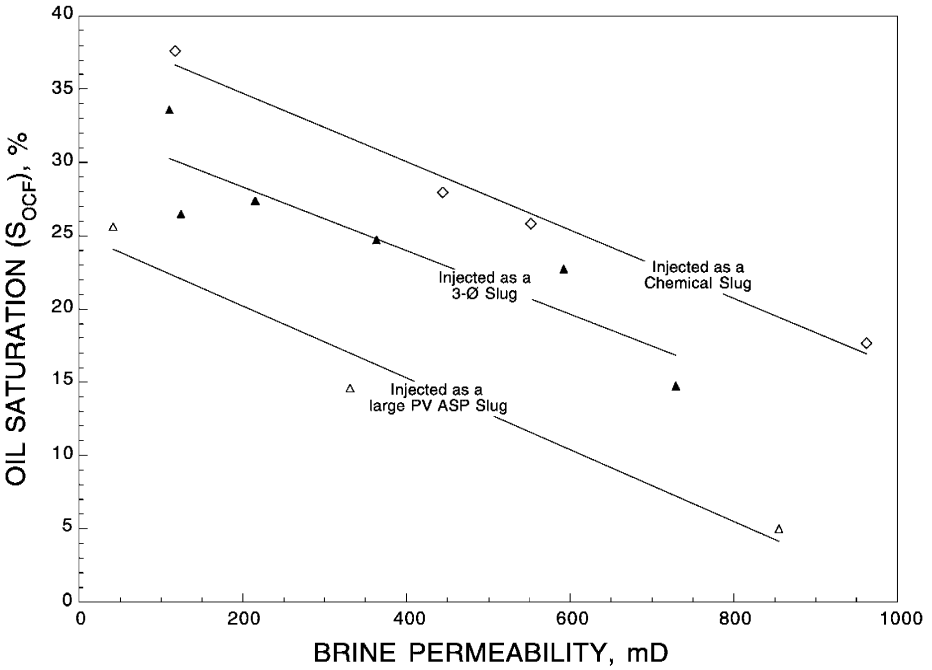

Figure 3–3 **Comparison of Oil Saturation (S_{ocf}) vs. Brine Permeability. Experiments were conducted using (a) straight chemical slugs, (b) 3-Ø slugs, and (c) large PV ASP slugs.**

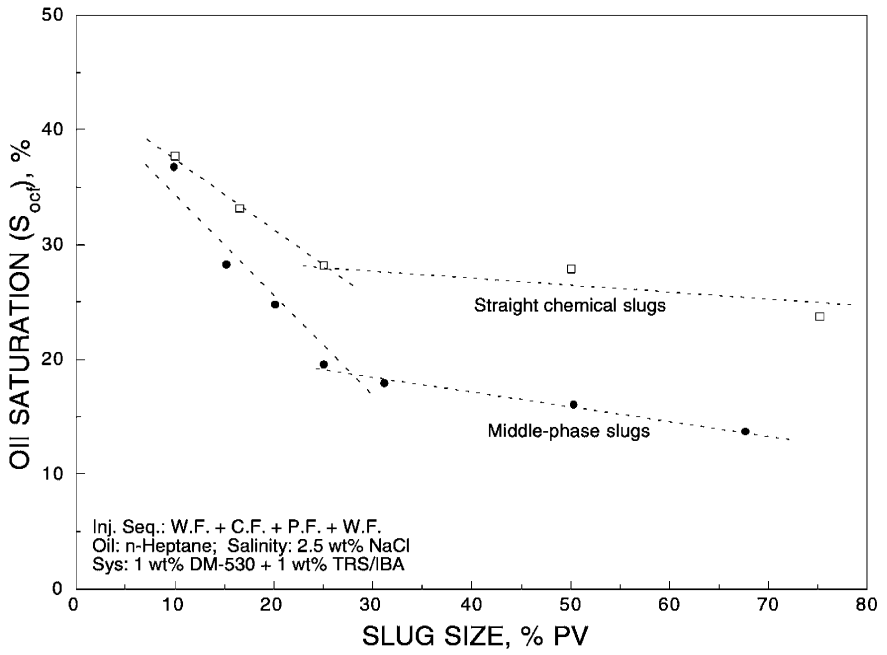

Figure 3–4 **Comparison of Oil Saturation (S_{ocf}) vs. Chemical Slug Size.**

Figure 3–4 shows a comparison plot of the post-test oil saturation vs. percent pore volume of chemical slug injected, for both middle-phase slug and straight chemical slug injections. For both cases tested, the influence on oil recovery was significant for slug sizes less than 25% PV. Results of the middle-phase slug tests showed that much lower oil saturation levels could be achieved than for the straight chemical slug experiments, at comparable slug sizes. The results for both cases indicate an optimal chemical slug size of about 25% PV. Greater oil recoveries can be achieved at the expense of using larger treatment volumes.

The difference in oil recovery with the middle-phase slugs and the straight chemical slugs was is significant. Although the chemical system was optimized from earlier screening efforts, an explanation is required to account for the difference in displacement behavior. The formulation injected as a straight slug may not be capable of sustained propagation of an oil bank, particularly for the relatively short contact time between fluids in situ. This behavior was very much in contrast to the CT-observed behavior using preequilibrated, middle-phase slug that preferentially "banked" oil (Llave et al. 1994). For comparison, CT-monitored coreflooding experiments were conducted using straight chemical slug injection. These were compared to observations made with the middle-phase slug injection tests reported earlier.

The results of the CT-monitored displacement experiments using the straight slugs showed very good displacement of the oil remaining after waterflood during the surfactant slug injection cycle (first 0.25 PV chemical). The residual oil saturation was relatively low in the chemical swept zone. This indicated that the chemical system was suitable for displacing the target hydrocarbon. Oil displacement and propagation was not sustained throughout the injection sequence, however. The buildup of oil saturation ahead of the surfactant slug injection stalled during injection of the polymer mobility control slug; and fingering of the injected fluids was evident as the main bulk of the front failed to propagate. Additional coreflooding experiments were then conducted to determine an injection strategy that can be used to improve the system's oil displacement potential. The images generated during the CT-monitored experiments are presented and discussed in a later section.

3.2.3 Chemical Screening Tests

Possible reasons for retardation of the front observed in the CT-monitored displacement experiments included:

1. Insufficient mobility control to mobilize the front
2. Loss of active chemicals due to adsorption or phase trapping
3. Surfactant-polymer incompatibility
4. In-situ elevated viscosity levels of the resulting middle-phase

Elevated viscosities was discounted based on results from earlier studies that indicated fairly low resulting viscosities for the middle-phase slugs. In addition, routine viscosity measurements for the polymer system (1,000 ppm biopolymer) indicated favorable mobility ratios. Surfactant-

polymer incompatibility was discounted based on the results of earlier screening studies. Results of PIT and salinity scans in the presence of the biopolymer are presented in Figures 3–5 and 3–6 (Llave et al. 1994). These plots show the conductivity vs. temperature for the solutions containing 500 and 1,000 ppm polymer. The solution behaved similarly to the surfactant system without polymer added (Figure 3–7). Figure 3–8 indicates only a slight difference/shift in the presence of the polymer. The results of salinity scans also supported these observations. No significant shift in solution behavior during the coreflooding tests was expected for the range of polymer concentrations tested. Additional information on these tests was presented earlier (Llave et al. 1994).

3.2.4 Polymer Concentration

Efforts to determine the effect of polymer loading on displacement behavior were undertaken. Displacement experiments were conducted using different polymer concentrations for the mobility control slug, injected immediately after a nonequilibrated chemical slug. These experiments were conducted for polymer concentrations of 500, 1,000, 1,500, and 2,000 ppm. Prior to these experiments, baseline information indicated inadequate propagation of the oil bank using 1,000 ppm polymer concentration with the result that significant amounts of oil were left in the core. These experiments provided an indication of the optimal polymer concentration for this chemical system. The results of these experiments were also compared to the salinity gradient approach, with the polymer slug formulated with fresh water, followed by a brine slug. Figure 3–9 shows a plot of the final oil saturation vs. polymer concentration. The plot shows the

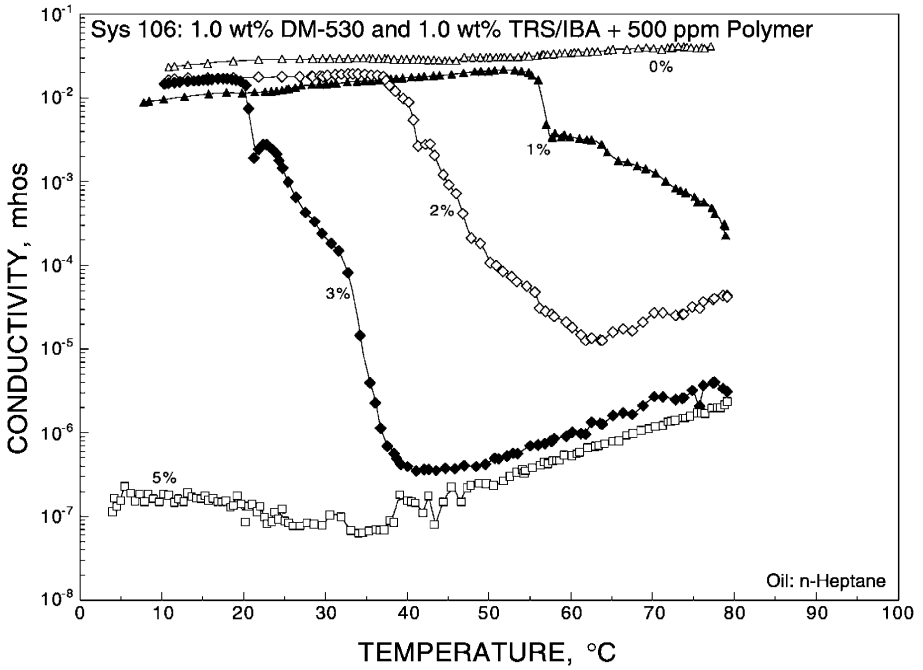

Figure 3–5 Phase Inversion Temperature (PIT) for 1.0 wt% DM-530 + 1.0 wt% Petronate L/IBA with n-Heptane and 500 ppm Polymer.

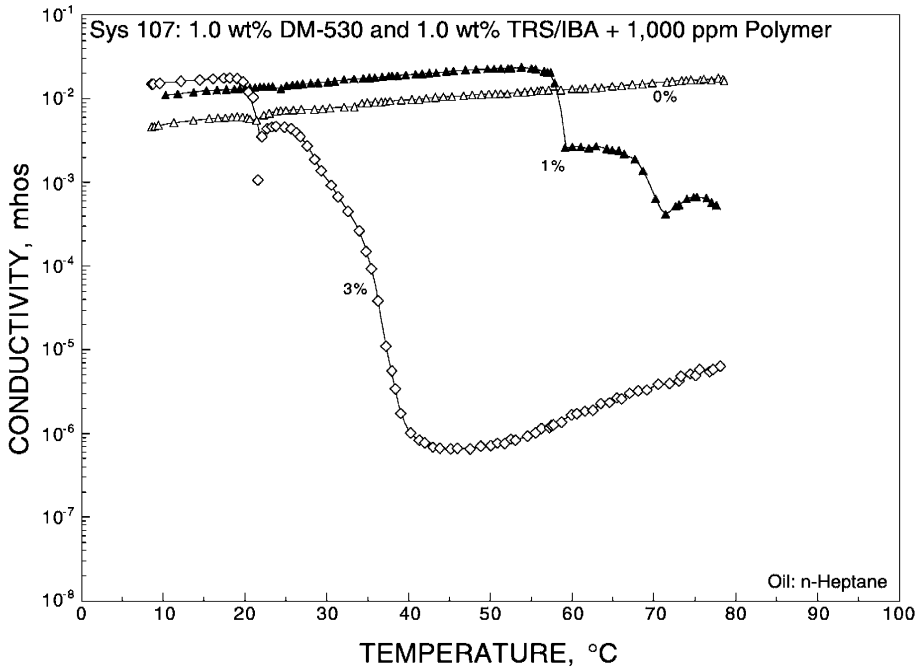

Figure 3–6 **Phase Inversion Temperature (PIT) for 1.0 wt% DM-530 + 1.0 wt% Petronate L/IBA with n-Heptane and 1,000 ppm Polymer.**

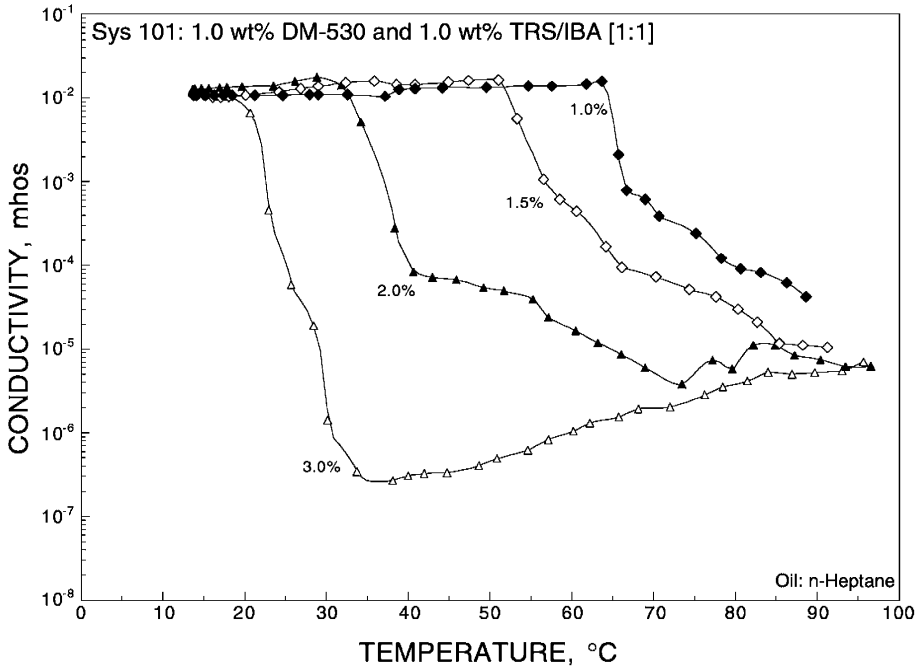

Figure 3–7 **Phase Inversion Temperature (PIT) for 1.0 wt% DM-530 + 1.0 wt% Petronate L/IBA [1:1] with n-Heptane.**

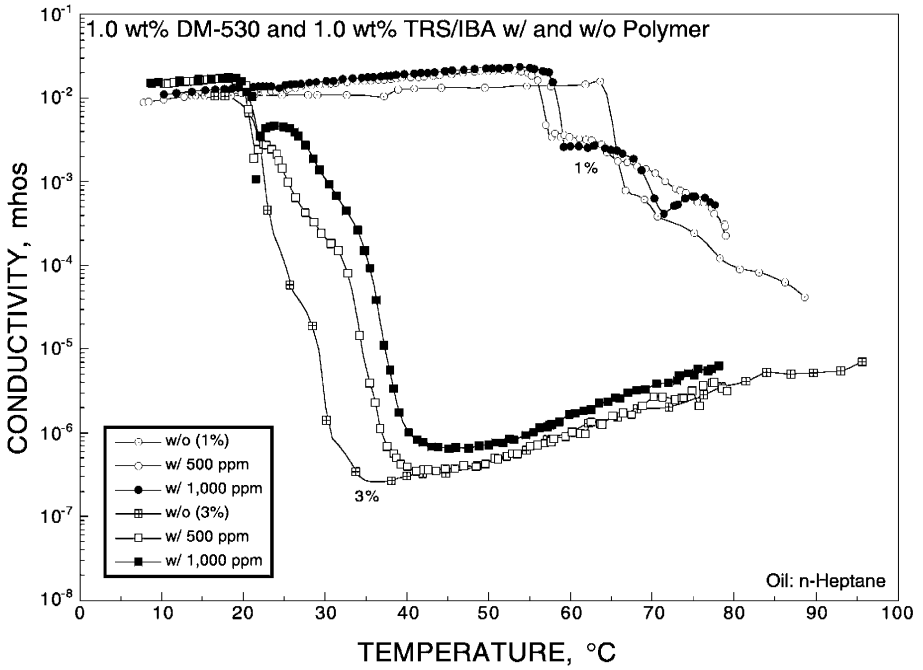

Figure 3–8 Effect of Polymer Loading on Phase Behavior of DM-530 + Petronate L/IBA System with n-Heptane.

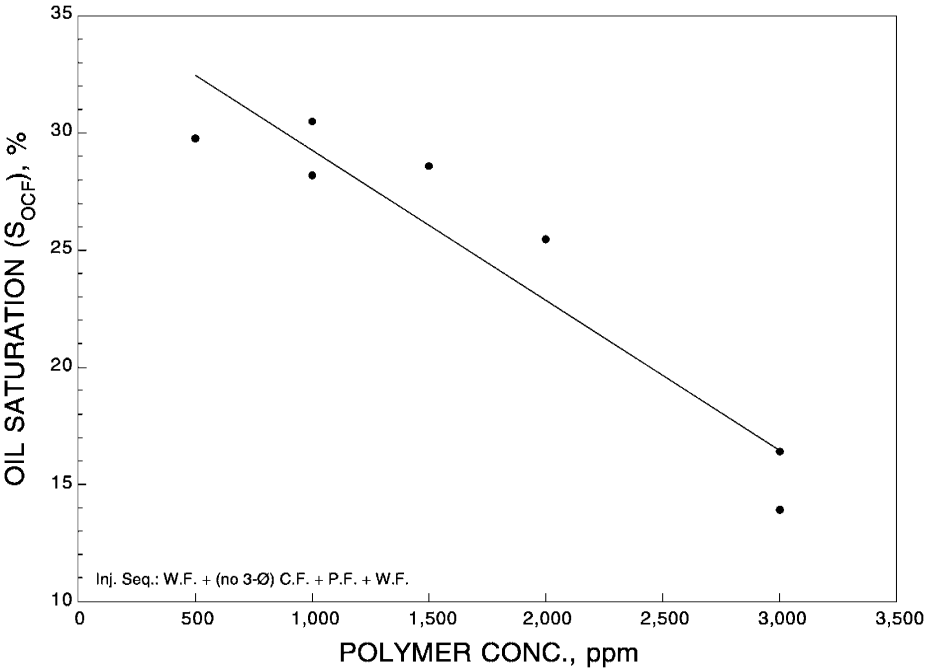

Figure 3–9 Residual Oil Saturation vs. Polymer Concentration.

significance of polymer loading of the on oil displacement. The experiment using 3,000 ppm polymer was conducted to determine the effect of this concentration level on oil recovery. It would be uneconomical to utilize high polymer concentrations in field applications, however.

These results were compared with the results from salinity gradient experiments using 1,000 ppm biopolymer. The oil recovery from the salinity gradient experiments was much higher. The overall results support the following trend:

500 ppm ≤ 1,000 ppm < 1,500 ppm < 2,000 ppm < salinity gradient @ 1,000 ppm < 3,000 ppm

Application of a salinity gradient during polymer and brine injection for nonequilibrated chemical slug injection improves the oil displacement potential of the chemical system used in this study. Similar efforts will be undertaken to improve the potential of the middle-phase slug injection scheme.

Figure 3–10 and 3–11 show plots of the oil cut and the oil recovery, respectively, versus pore volume injected for different polymer concentrations. The injection sequence in these experiments involved:

1. Brine saturation of the dry core
2. Brine displacement by oil to initial oil saturation (S_{oi})
3. Oil displacement by brine to residual oil saturation after waterflood (S_{orw})
4. Straight chemical slug injection
5. Polymer injection for mobility control - 1.0 PV total
6. Follow-up brine as drive fluid - 1.0 PV total

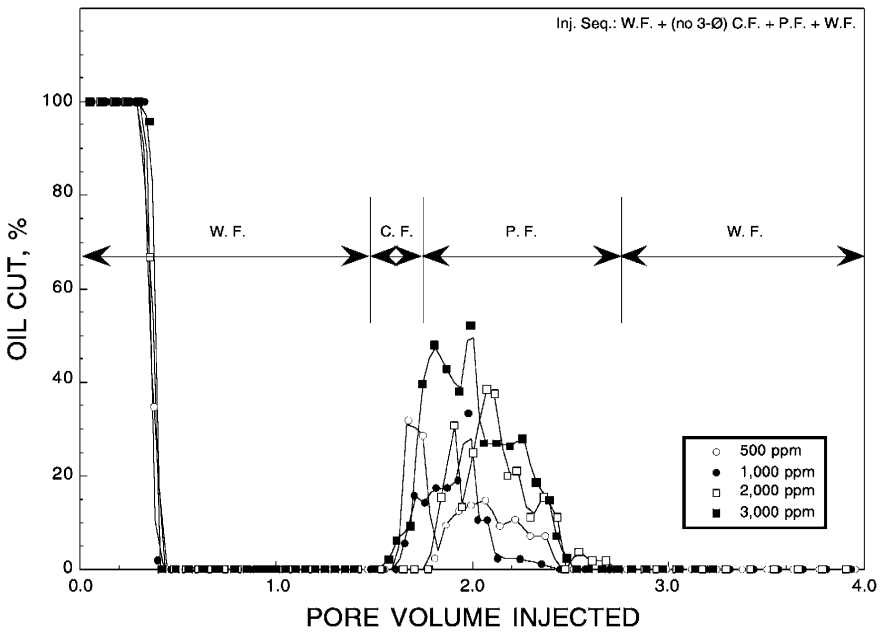

Figure 3–10 Oil Cut vs. Pore Volume Injected Using Different Polymer Concentrations.

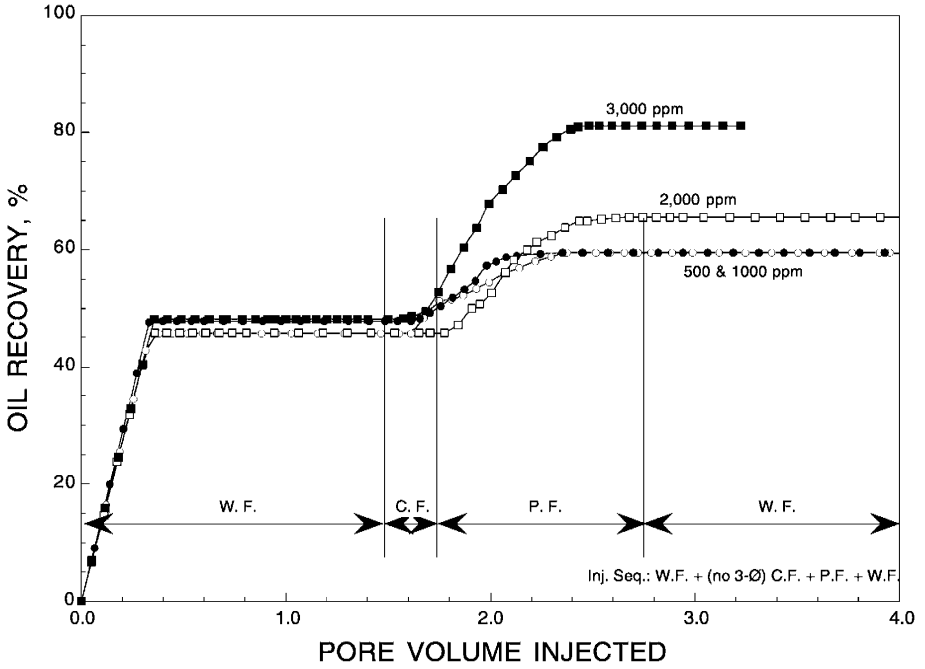

Figure 3–11 Oil Recovery vs. Pore Volume Injected Using Different Polymer Concentrations.

Figure 3–10 shows the oil cut during the progress of the experiments. The breakthrough times for the initial waterflood were comparable for all the tests conducted. Chemical slug was initiated after injection of 1.5 ± 0.2 PV. For each test, about 0.25 PV chemical slug was injected, followed by the polymer and the follow-up brine. Oil production was initially observed after approximately 0.25 PV fluid injection. Total oil production when using 500 and 1,000 ppm polymer concentration was very similar. The oil cuts (maximum oil cut of 30%) were not as large as those observed with the 2,000 and 3,000 ppm polymer experiments (>40% oil cut), and total production was lower for the lower concentration experiments. Oil production almost ceased by the end of the 1.0 PV polymer slug injection.

Figure 3–11 compares oil recovery for different polymer loadings. This plot shows the same displacement trend during each waterflood cycle. Oil recovery at water breakthrough was about 45% to 50%, at about 0.40 PV injected. The differences were evident at the later stages of the surfactant injection and at the onset of the polymer injection. Higher polymer concentration experiments yielded better oil recovery, 65.6% and 81.1% of original-oil-in-place (OOIP), respectively. Both the 500 and 1,000 ppm polymer concentrations yielded much lower, but comparable ultimate oil recoveries, about 59.5% OOIP. The difference in the latter two experiments can be seen in the rate of oil recovery vs. PV, particularly in the early stages of the polymer injection. The 1,000 ppm polymer concentration (solid circles, Fig. 3–11) indicated much faster approach to residual conditions, than for the 500 ppm polymer concentration (hollow circles, Fig. 3–11). Improved oil production response is favored by increased polymer loading.

Results of the 1,500 ppm polymer concentration (not shown) was only slightly better than the two lower concentration runs. These result indicate the need for a minimum polymer loading (minimum mobility threshold) for improved displacement.

3.2.5 CT-Imaging of Mixed Surfactant Coreflood Experiments

In this section, several oil recovery experiments are described that used non-invasive CT-imaging techniques to monitor fluid front propagation. In these studies, the oil was tagged with iododecane to provide an increased X-ray absorption contrast between the oil and injected fluids.

Figure 3–12 shows a series of plots of the progress of one of the CT-monitored coreflooding experiments (Experiment 23). This particular experiment was conducted in low permeability Berea core (≈ 100 md) containing variable permeability layers that affected the fluid movement during the test. The injection sequence in this experiment involved:

1. Brine saturation of the dry core
2. Brine displacement by oil to S_{oi}
3. Middle phase (3-Ø) slug injection
4. 1,000 ppm polymer injection for mobility control - 1.0 PV total
5. Follow-up brine as drive fluid - 1.0 PV total (fluid injection was from left to right)

The core was CT-scanned during different stages of the experiment. Figure 3–12a shows the fully oil saturated core, with an average initial oil saturation of 61.8% (by material balance). The image shown in Figure 3–12a indicates the presence of horizontal streaks of relatively high oil saturation throughout the length of the core. The lighter images indicate higher oil saturation. Uneven oil saturation was observed in this CT-generated image. The core porosity/permeability contrast directly affected the resulting oil saturation distribution and subsequent displacement behavior. Figure 3–12b shows the scan taken after injecting the 0.25 PV chemical slug. The areas contacted, by the chemical slug showed good frontal sweep, indicative of favorable oil recovery, with some degree of override. One thing to note about this experiment was that there was oil present (approximately 22%, n-heptane) in the slug injected as middle-phase chemical system. The image may show almost zero saturation (in terms of the tagged oil component) in areas contacted but some untagged oil, introduced during injection of the 3-Ø slug, remained. Figures 3–12c and 3–12d show the scans taken after 0.25, and 0.87 PV polymer slug injection, respectively. Although the surfactant appeared to invade most areas of the injection end, significant areas of preferential polymer injection are noted in these scans, even as early as 0.10 PV polymer slug injection. Polymer breakthrough was observed in Figure 3–12c, after 0.25 PV polymer slug was injected. The degree of nonuniform sweep can be directly correlated with the presence of high oil saturation streaks shown in Figure 3–12a. Figure 3–12e was taken at the end of the experiment, after 1.0 PV of untagged brine was injected as a drive fluid. The final image

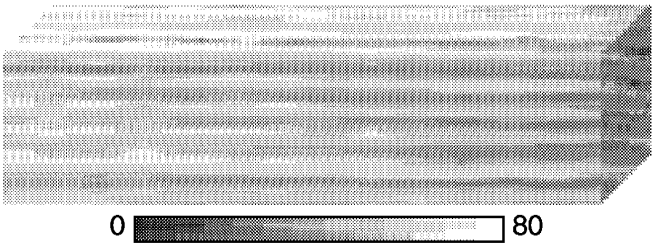

(a) Oil saturated core, Soi

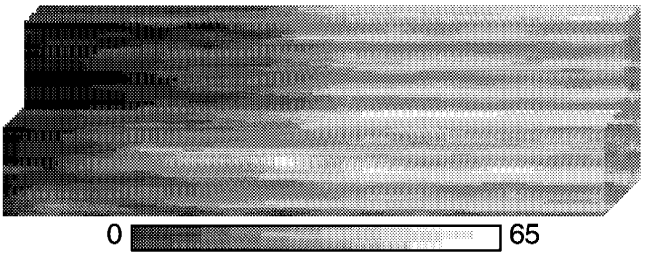

(b) After 0.25 PV 3-Ø chemical slug injection

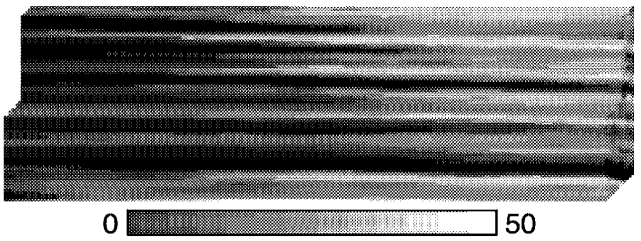

(c) After 0.25 PV polymer slug injection

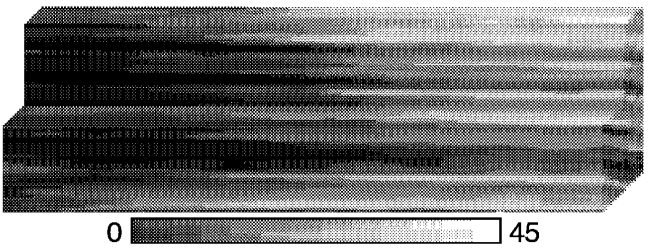

(d) After 0.87 PV polymer slug injection

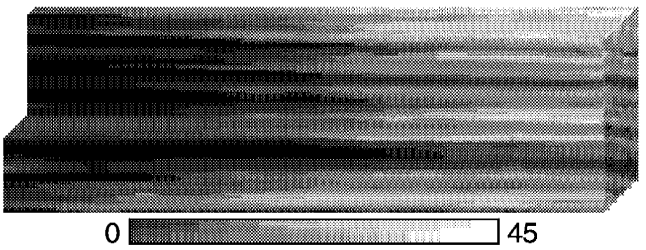

(e) Final oil saturation after experiment

Figure 3–12 CT-monitored Flow Profile for Experiment 23 (L to R). Color bar represents% oil saturation.

shows excellent sweep of about 1/4 of the front-end of the core. The areas contacted by the chemical slug were well swept, but the remaining 3/4 sections of the core showed considerable bypassed oil. Relatively high oil saturations can be observed in the unswept section. The final average oil saturation of the core was about 26.75% for a recovery efficiency close to 57%. The results demonstrate the effect of permeability heterogeneity on oil displacement, A comparison can be made with experiments reported by Llave et al. (1994) in high permeability cores under similar conditions.

Figure 3–13 shows the plots for Experiment 24. This experiment was conducted using the straight chemical slug injection in a high permeability Berea sandstone core. (The chemicals were not preequilibrated with oil before injection into the core.) The injection sequence involved:

1. Brine saturation of the dry core
2. Brine displacement by oil to S_{oi}
3. Straight chemical slug injection
4. 1,000 ppm polymer injection - 1.0 PV total
5. Follow-up brine as drive fluid - 1.0 PV total

The core was CT-scanned during the experiment. Figure 3–13a shows the fully oil saturated core (S_{oi}= 76%) and indicates uniform oil distribution in the core. Figures 3–13b and 3–13c show the scan taken during injection of an untagged chemical slug (at 0.25 PV) and the polymer slug (after 0.50 PV), respectively. Figure 3–13b shows that areas contacted by the chemical slug had significantly lower oil saturations, indicative of favorable displacement. After injection of 0.5 PV polymer slug (Fig. 3–13c), some of the oil bank (lightest color) has progressed through the core. Low oil saturations (dark areas), however, did not appear to extend much beyond the initial saturation reduction achieved during the chemical injection. Figure 3–13d shows the residual saturation after the follow-up brine. Only small changes in the oil saturation distribution, as shown in Figure 3–13c, can be detected for the poorly swept portion of the core. As mentioned in an earlier discussion, the oil appeared to stall mid-way through the core resulting in relatively poor oil recovery. In this case, the average final oil saturation was high at about 36.5%.

Figures 3–14 to 3–16 (experiments 42, 44, and 48) show a series of the CT images for the experiments using different polymer loadings, 1,500, 2,000 and 3,000 ppm, respectively. All these experiments were conducted under similar conditions, in high permeability (750 to 900 md range) Berea sandstone core using nonequilibrated chemical slugs (0.25 PV). The injection sequence in these experiments involved:

1. Brine saturation of the dry core
2. Brine displacement by oil to S_{oi}
3. Brine injection to S_{orw}
4. Straight chemical slug injection
5. Polymer injection for mobility control of different concentrations - 1.0 PV total
6. Follow-up brine as drive fluid - 1.0 PV total

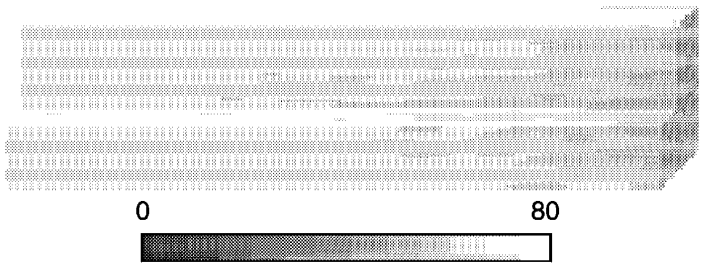

(a) Oil saturated core, S_{oi}

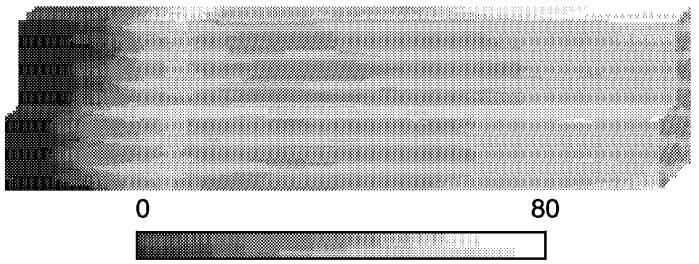

(b) After 0.25 PV straight chemical slug injection

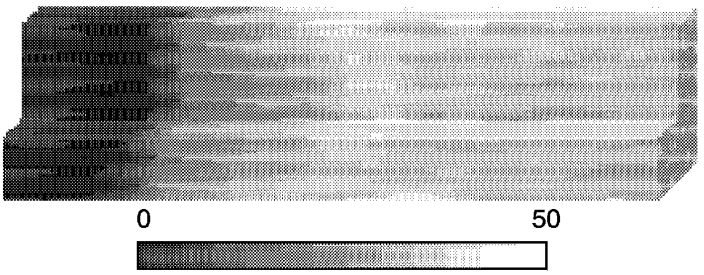

(c) After 0.5 PV polymer slug injection

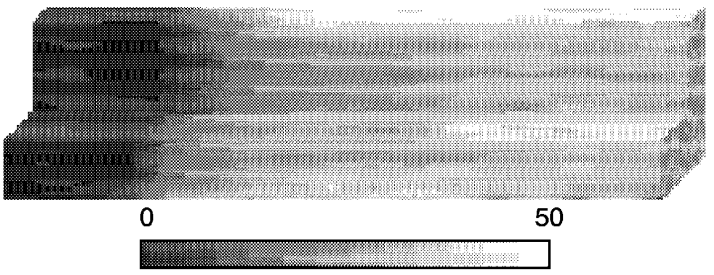

(d) Final oil saturation after experiment

Figure 3–13 CT-monitored Flow Profile for Experiment 24 (L to R). Color bar represents% oil saturation.

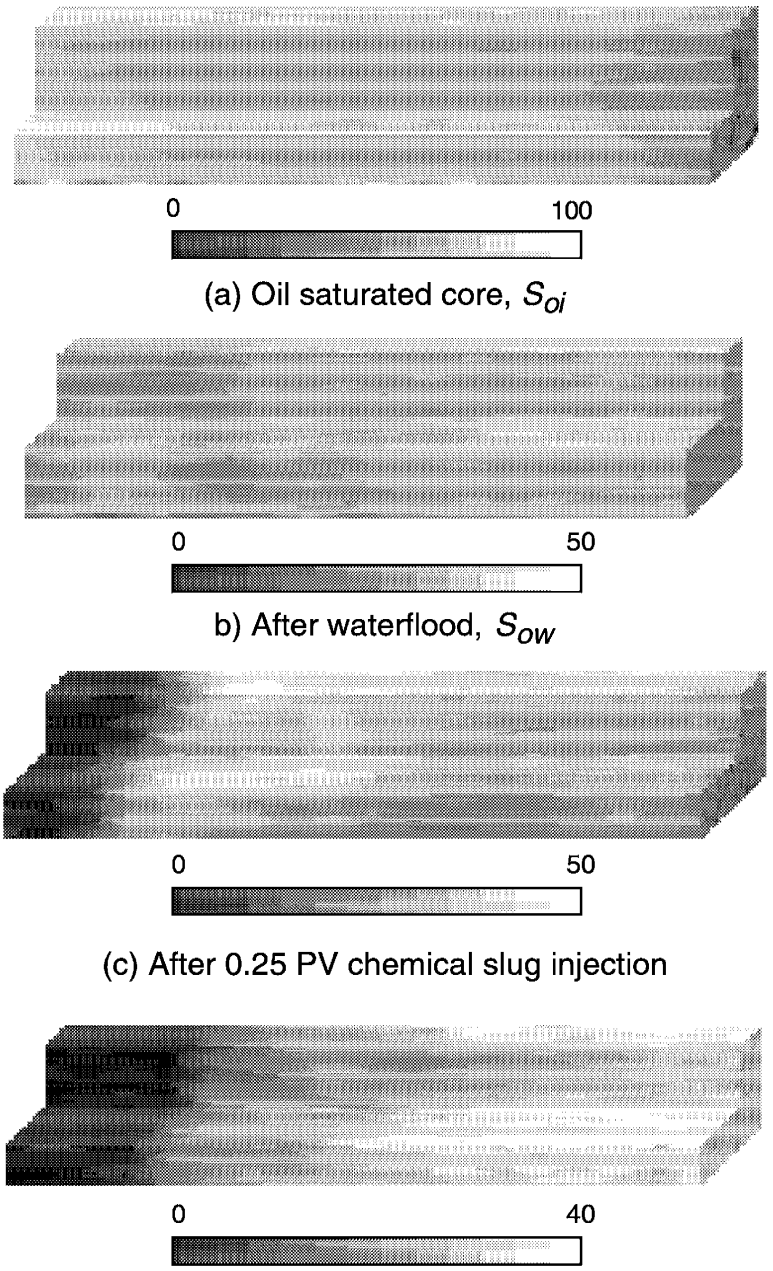

Figure 3–14 **CT-monitored Flow Profile for Experiment 42 Using 1,500 ppm Polymer. Gray scale represents% oil saturation.**

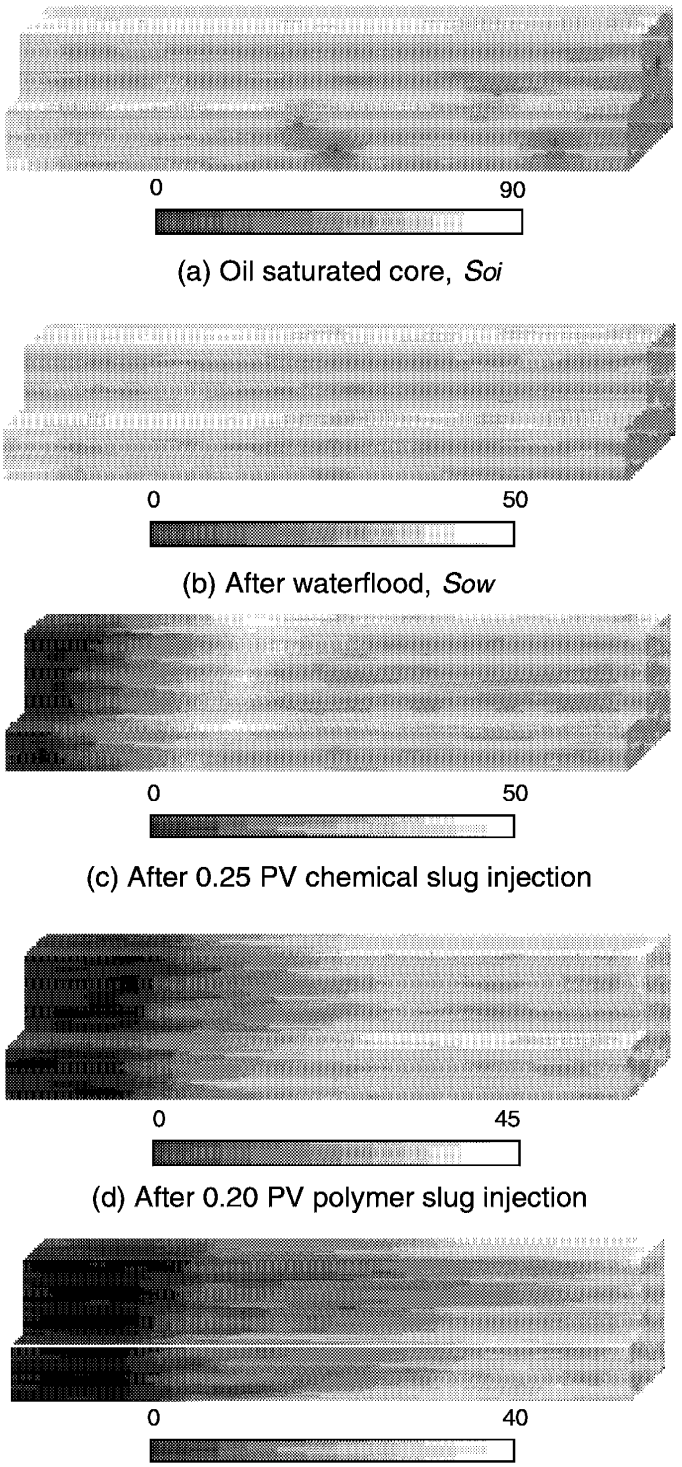

Figure 3–15 CT-monitored Flow Profile for Experiment 44 Using 2,000 ppm Polymer. Color bar represents% oil saturation.

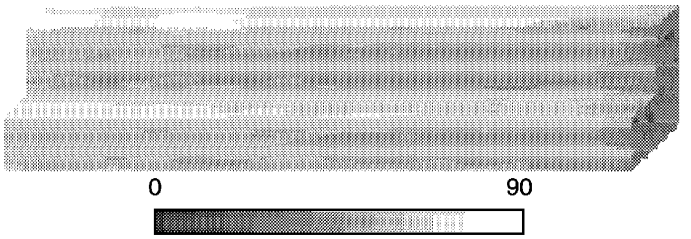

(a) Oil saturated core, *Soi*

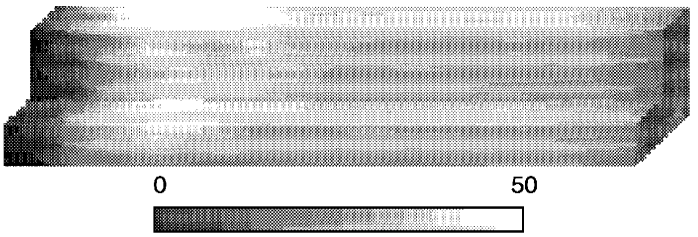

(b) After 0.25 PV chemical slug injection

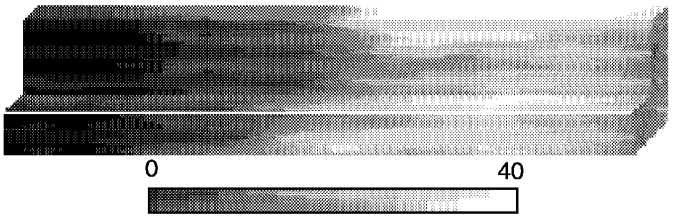

(c) After 0.30 PV polymer slug injection

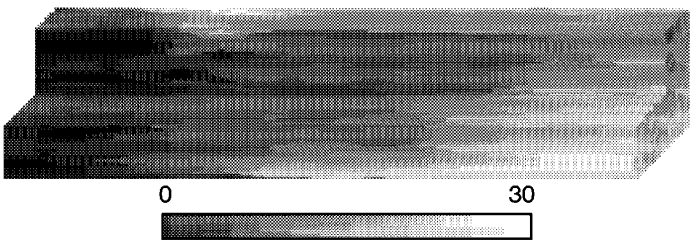

(d) After 0.60 PV polymer slug injection

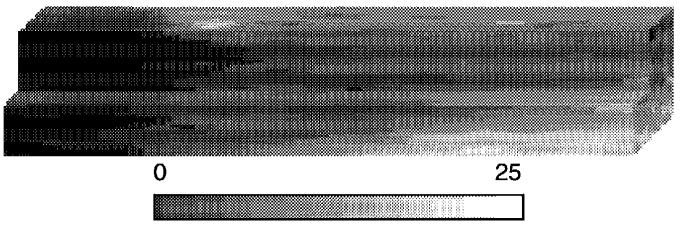

(e) After 1.0 PV polymer slug injection

Figure 3–16 CT-monitored Flow Profile for Experiment 48 Using 3,000 ppm Polymer. Color bar represents% oil saturation.

Figures 3–14a, 3–15a and 3–16a show the fully oil saturated cores, with average initial oil saturation of 72.9%, 71.6%, and 73.0%, respectively. Reasonably uniform saturations can be observed in these scans, with some slight difference noted for Experiment 44 (Fig. 3–15a) in the middle section of the core. After the waterflood stage, the oil saturations were comparable. Figures 3–14b and 3–15b (waterflood for Experiment 48 is not shown) all show uniform oil saturations after brine injection to residual oil saturations of 34.5% and 40% (36.0% for Experiment 48), respectively. Changes after injecting 0.25 PV of straight chemical slug was also similar. These images (Figs. 3–14c, 3–15c and 3–16b) show that the areas contacted by the chemical slug exhibited very good frontal sweep and favorable oil movement. The moving oil bank can be observed in these figures. The three experiments were comparable at this stage of the experiment. Similar response was observed for Experiment 45, using 500 ppm polymer concentration (not shown in the figures).

Oil saturation differences were observed during the polymer injection sequence. (see Figs. 3–14d, 3–15d and 3–16c to 3–16e). Figure 3–14d for Experiment 42 using 1,500 ppm loading shows relatively ineffective movement of the displacement front. Relatively high oil saturation remained in the core, 28.6%, which was only slightly better than the 500 ppm experiments (29.8%). Figure 3–15d for Experiment 44 (2,000 ppm) shows much improved displacement of the front. The CT-images indicated that about half of the core was swept, with the average final oil saturation of 25.5%. Figures 3–16c through 3–16e, for Experiment 48 (3,000 ppm), show the most significant improvement in displacement of the front. The whole core was almost swept. At this stage, a "wedge-like" region with some slightly higher oil saturations can be observed, indicative of some degree of override occurring about 1/3 from the end of the core. The average final oil saturation from this experiment was 16.4%.

The results of the CT-monitored experiments indicated the injected chemical slugs did not provide a sufficient "bank" to mobilize and produce oil. This case was fairly prevalent with the use of nonequilibrated chemical slugs. The chemical system was effective only to the extent of the pore volume swept by the active surfactant. Subsequent polymer injection, at relatively low concentration levels (1,000 ppm polymer concentration), was not effective in propagating the bank, resulting in poor oil recovery. Higher concentration polymer slugs, which resulted in improved mobility, banked and produced more oil. Both preequilibrated (middle-phase) chemical injection and a salinity gradient injection strategy were effective at lower polymer concentration levels. The results suggest that development of sustained favorable phase behavior is required to minimize polymer loading requirements.

More detailed studies are necessary to address several issues which include: (1) evaluation of the in situ phase behavior difference mixed surfactant systems; (2) investigation of improved mobility control methods; and (3) comparison of phase behavior screening and coreflooding displacement methods to evaluate chemical IOR systems.

3.3 CT-Imaging and Simulation Studies of a Surfactant/Polymer IOR System

3.3.1 Description of Experiment

A micellar surfactant-cosurfactant-polymer chemical flooding experiment (CT-CF 12) was conducted in relatively uniform, high permeability Berea sandstone core. Oil saturation distributions during chemical injection were determined using CT imaging. The objective of the experiment was to compare the CT saturations with oil saturations generated using the UTCHEM chemical simulator. The chemical system and experimental protocol was chosen for a number of reasons including:

- Good oil recovery characteristics of the chemical system
- Extensive characterization of the phase behavior of the fluids
- Simulation of oil saturation distributions within porous media during chemical flood has not been done
- Availability of experimental and simulated oil production data in the literature (Camilleri et al. 1987a) that can be used to compare and verify the results from this study

The minipermeameter was used to measure the air permeability of the core for the core inlet and outlet faces and along each side. The core was then encased in epoxy and saturated with brine. The permeability and the porosity of the whole core was then measured. The uniformity of the core was determined using a CT tracer test, with the brine tagged with sodium iodide (NaI). This was the only stage of the experiment where the aqueous phase was tagged for the CT. During the chemical flood, the oil was tagged with iododecane. Tagging the aqueous phase during the chemical flood would adversely affect the phase behavior of the surfactant-oil system.

The core was then oil flooded to residual brine saturation followed by a waterflood to residual oil saturation. Table 3–2 summarizes core properties and permeability values for different fluid saturations.

The chemical system used in test CT-CF 12 is listed in Table 3–3. The experiment was conducted at ambient temperature using an oil tagged with iododecane to provide X-ray absorption contrast between the oil and aqueous fluids in the core. The main difference between the phase behavior of the surfactant and tagged oil system to that of the surfactant and untagged oil was a slightly lower optimal salinity (1% NaCl). (The optimal salinity of the untagged oil system at ambient temperatures was 1.2% NaCl). This compares with the optimal salinity (0.95% NaCl) observed for n-decane and the surfactant system used in a laboratory and simulation study described in the literature (Camilleri et al. 1987a). Camilleri's chemical system contained isobutyl alcohol rather than isopropyl alcohol. In addition, his test was conducted at 30°C. These differences appeared to cause little change in oil recovery, however.

Table 3–2 Core Properties and Permeabilities for CT-CF 12

Core Properties		
Core dimensions	**Value**	**Unit**
Height	5.3	cm
Width	5.25	cm
Length	26.0	cm
Bulk volume	723.6	cm^3
Pore volume	168.2	cm^3
Porosity	23.3	%
Initial permeability to brine	530	md
Oil permeability at 35% brine saturation	176	md
Brine permeability at 32% oil saturation	56	md

Table 3–4 summarizes the fluid injection sequence used to conduct the tracer and tertiary oil recovery test. A CT scan was conducted after each injection step. Sixty-three CT slices, each 4 mm in length, described the core. Each CT pixel represented an volume of the core 0.5 x 0.5 x 4 mm. Fluid effluent was collected using a fraction collector to monitor water and oil production with time. Simulation of the tracer test was conducted using several different simulators, BOAST, PC-GEL, and UTCHEM. Only UTCHEM could be used to simulate the chemical flood, however. Camilleri et al. (1987a) used UTCHEM to simulate pressure data and fluid production for the comparable experiment. Fluid saturation distributions within the core were not directly measured in Camilleri's study.

Table 3–3 Fluid Compositions Used During CT-CF 12 Chemical Flood Experiment

Fluids	Composition	PV Injected
Tracer test:		
Initial brine	3 wt% KCl	
Tracer	10 wt% NaI in 3 wt% KCl	0.205
Chemical flood:		
Initial brine	1.7 wt% NaCl	
Oil	80 wt%/20 wt% Decane/Iododecane	
Surfactant slug	3.0 vol% Petronate L (TRS 10-410) 3.0 vol% IPA 992-ppm Flocon 4800-CX (Xanthan biopolymer) 0.04 wt% NaCl	0.136
Polymer slug	1,000 ppm Flocon 4800-CX 0.04 wt% NaCl	1.39

Table 3–4 Fluid Injection and CT Imaging Sequence for CT-CF 12

	Operation	PV
	Tracer test	
1.	Dry core in encased in epoxy	
2.	Saturate core with 3% NaCl	5
3.	Inject Tracer - 10% NaI and 3% KCl	0.205
4.	Inject 3% KCl	0.260
5.	Inject 3% KCl	0.355
6.	Inject 3% KCl	0.204
7.	Inject 3% KCl	0.50
	Tertiary oil recovery experiment	
1.	Inject 1.7% NaCl	5
2.	Inject n-Decane/Iododecane	
3.	Waterflood to residual oil @7.3 ft/D	
4.	Inject surfactant slug @ 0.89 ft/D	0.136
5.	Inject polymer slug @ 0.89 ft/D	0.173
6.	Inject polymer slug	0.126
7.	Inject polymer slug	0.103
8.	Inject polymer slug	1.002

3.3.2 Core Characterization

A rectangular core plug was cut from a uniform, high permeability Berea sandstone core. Core dimensions are listed in Table 3–2. Air permeability variation along each side and ends of the sample were determined using the minipermeameter. Figure 3–17 shows the positions of the minipermeameter measurements. The permeability data is useful in determining the presence of major heterogeneities affecting fluid flow through the core and in constructing a permeability/porosity map for the simulator. Permeability variation along Sides 5 and 6 (the two ends of the core) are shown in Figure 3–18. The air permeabilities are relatively uniform across Side 6 but show a variation up to a factor of two across Side 5. (Based on the uniform measurements for Side 6, this end was selected as the injection end for the oil recovery experiment.) The permeability measurements along Sides 1 to 4 were lower than the end face permeabilities and were particularly low along Sides 1 and 2, as shown in Figures 3–19 and 3-20. The lower permeabilities may be indicative of reduced surface permeability from fines caused by handling, cutting, or abrasion since these sides were the original sides of the Berea sandstone block as received from the quarry. Future core handling procedures will be formulated to minimize surface damage during cutting and handling.

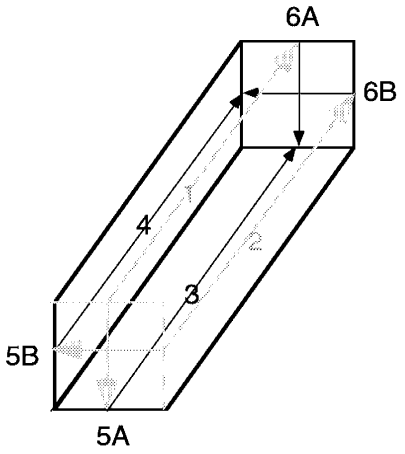

Figure 3–17 **Schematic of Core for Simulation of CT-monitored Chemical Oilflood Experiment, CT-CF 12.**

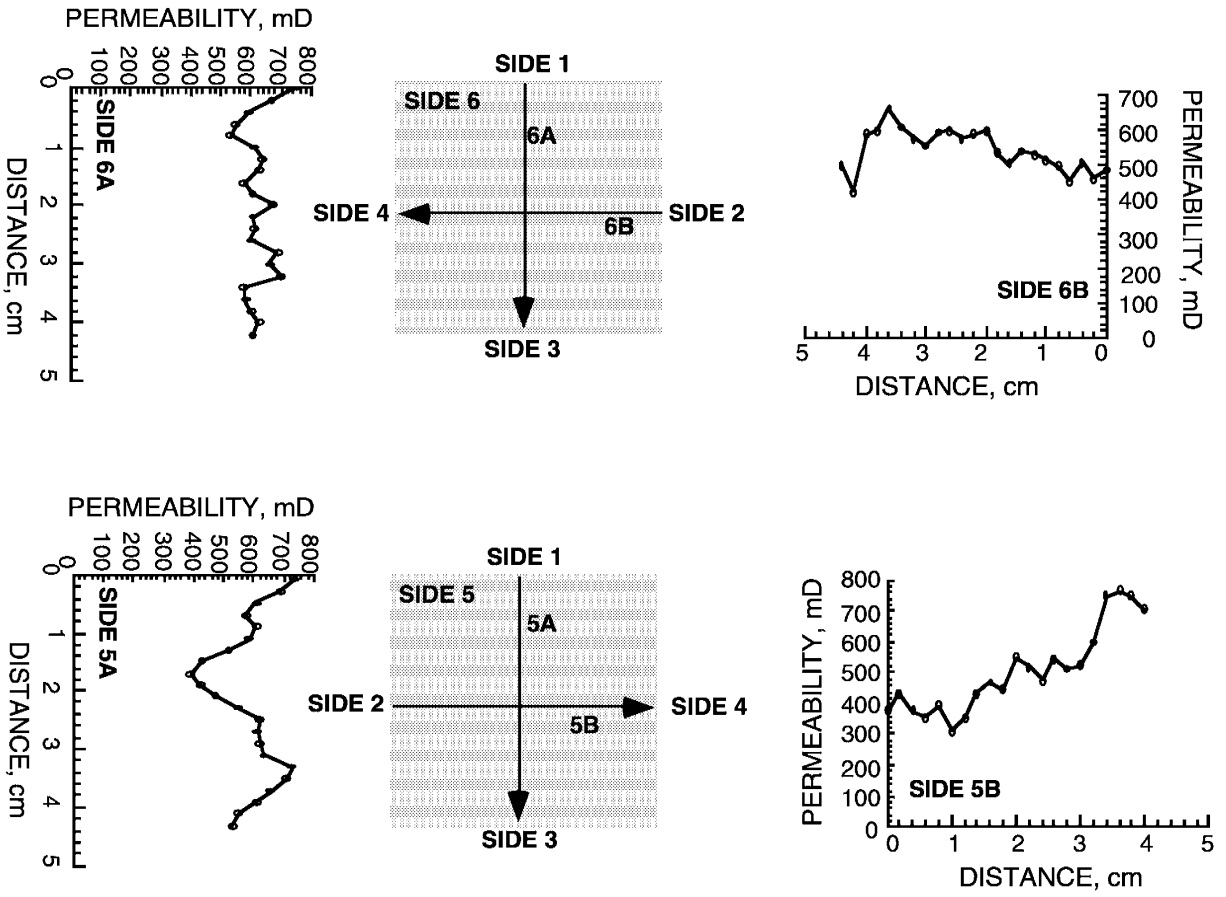

Figure 3–18 **Minipermeameter Permeability Measurements of the End Faces (Sides 5 and 6) of Core CT-CF 12.**

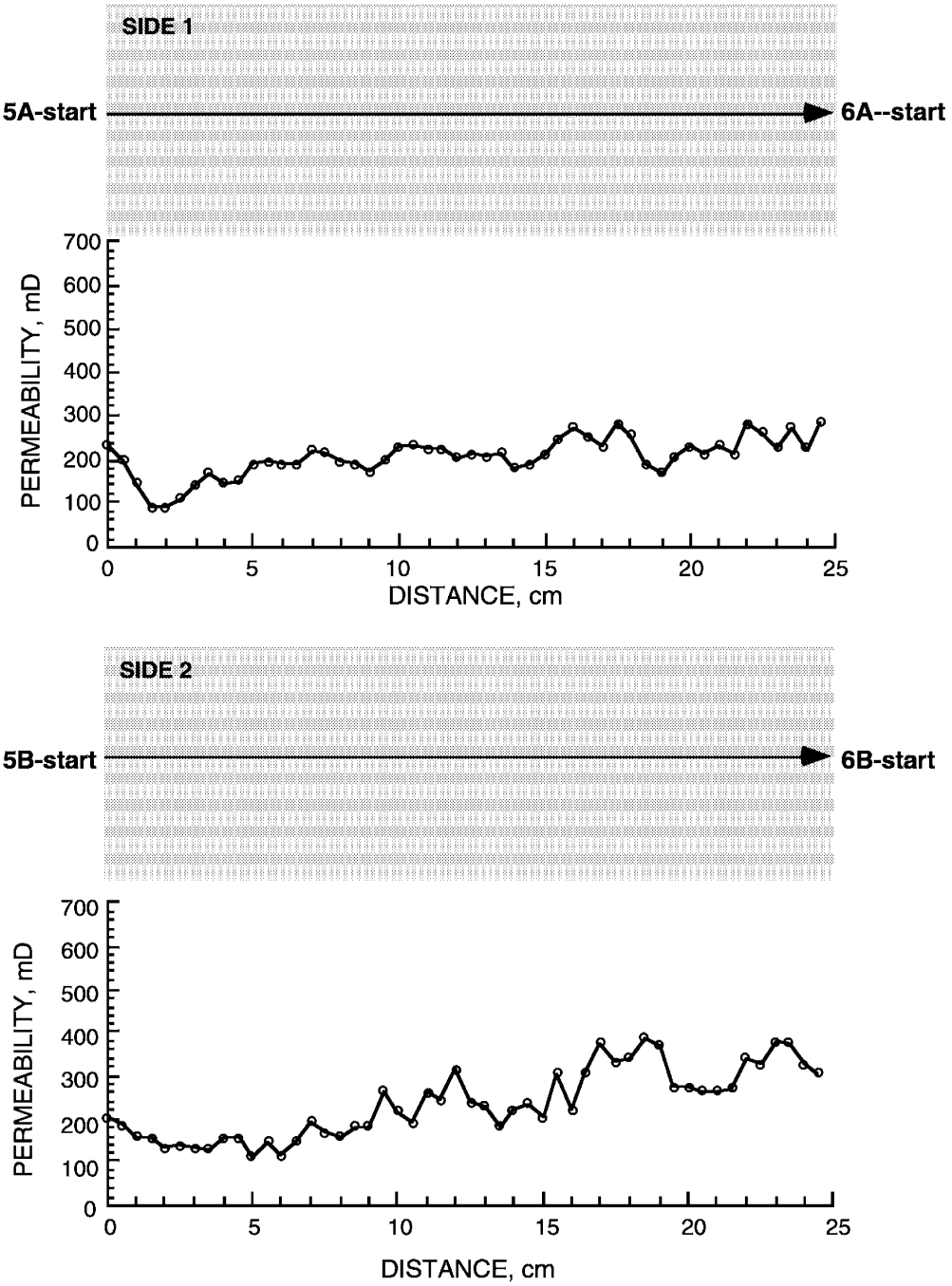

Figure 3–19 **Minipermeameter Permeability Measurements of Sides 1 and 2 of Core CT-CF 12.**

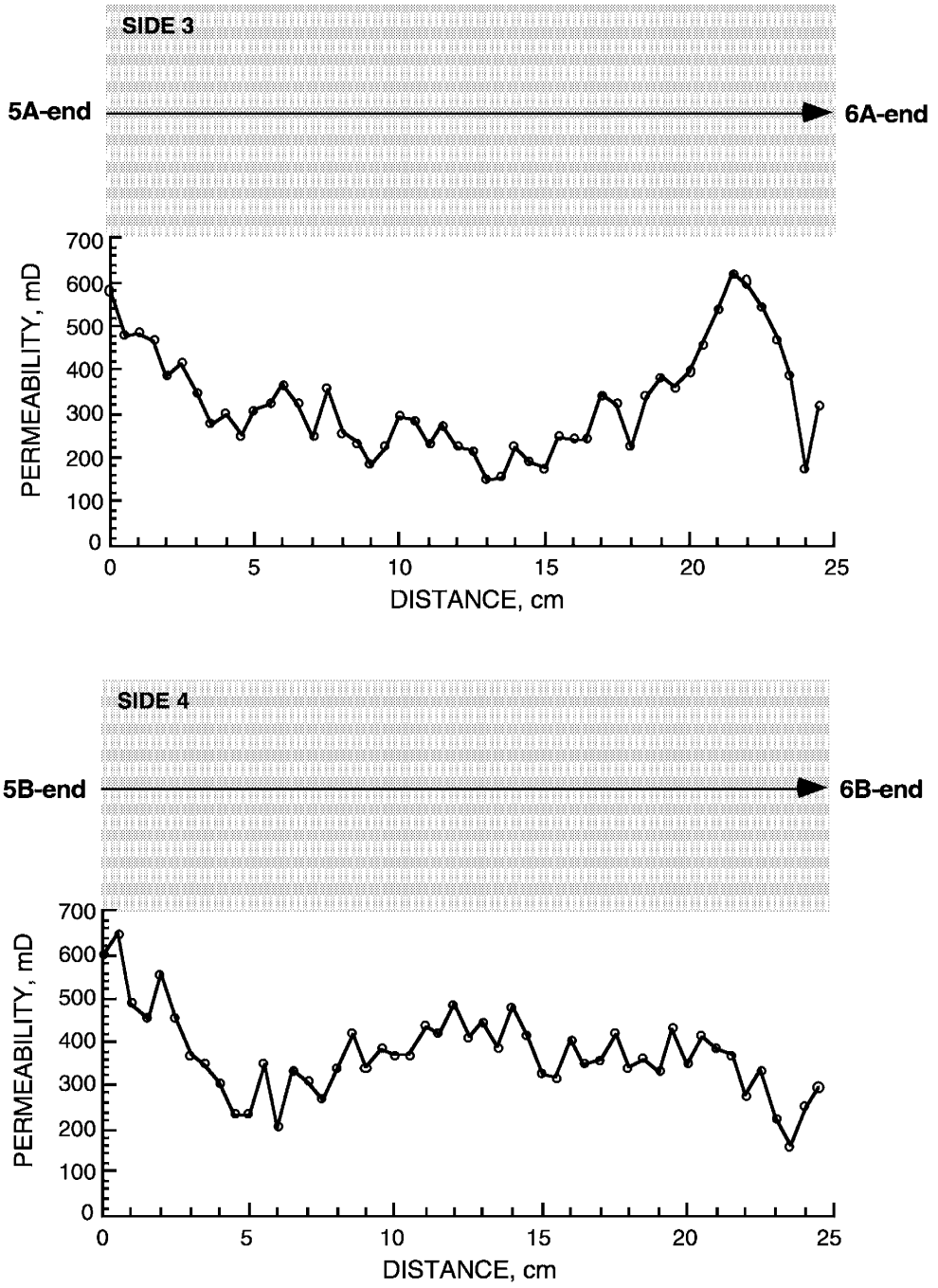

Figure 3–20 **Minipermeameter Permeability Measurements of Sides 3 and 4 of Core CT-CF 12.**

Separate samples of Berea sandstone core were selected and surface air permeabilities were measured using the minipermeameter. Thin sections to include the tested area were used to determine porosity by pore image analysis (PIA). Figure 3–21 shows the resulting permeability/porosity relationship. This correlation was used to determine a permeability map for sample CT-CF 12 from the porosity values generated by CT-imaging. Both the porosity and permeability maps were used in the simulators.

The CT-CF 12 core sample was then encased in epoxy and saturated with brine. The average porosity and permeability of the core was measured as 23.3% and 530 mD, respectively. This agrees closely with the permeability/porosity correlation shown in Figure 3–21.

CT images (140 x 140 pixels) were obtained for the dry and brine saturated core. Porosity values at each pixel were calculated by subtracting the dry image from the saturated image and dividing by the difference in the CT values for brine and air. Figure 3–22 shows the porosity map of a vertical slice down the middle of the core. The average porosity along the core (average porosity of each CT image), as shown in Figure 3–23, decreased slightly from one end of the core to the other (from end 6 to end 5).

A CT tracer test using brine tagged with 10% NaI was conducted to determine the fluid flow characteristics through the core. Table 3–3 lists the fluid injection schedule for the tracer test. Figure 3–24 shows the CT tracer profiles during the brine injection. Initially the fluid front was uniform, but as injection continued, gravitational effects could be observed due to differences in fluid densities. Tracer density was 1.10 g/mL, and brine density was 1.02 g/mL. No major core heterogeneities were observed for CT-CF 12. Simulation of the tracer movement through the core is described in a later section of this report.

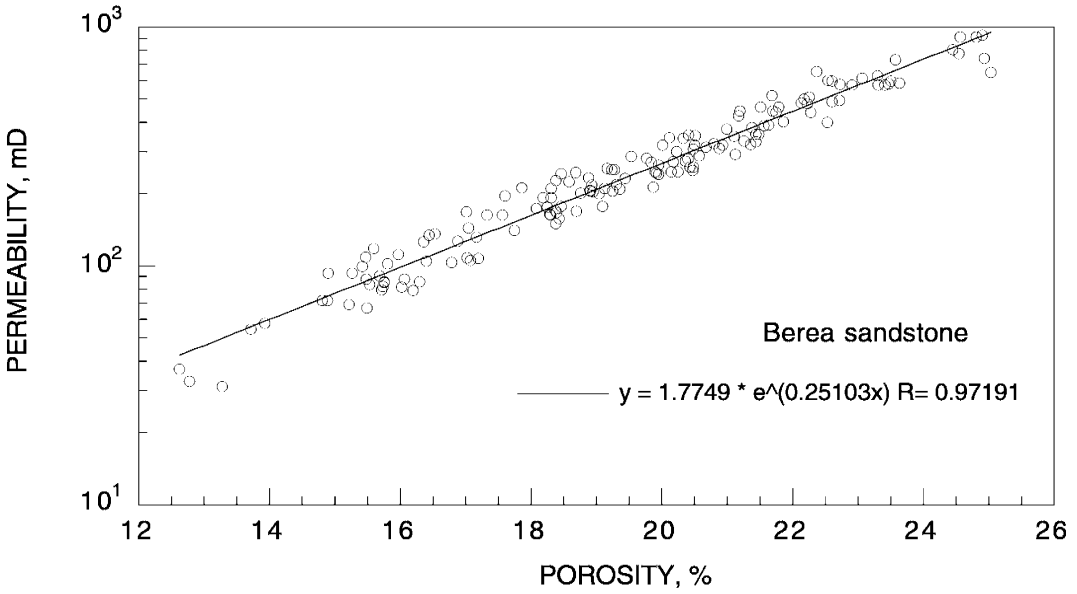

Figure 3–21 Permeability/Porosity Correlation for Berea Sandstone Core from Minipermeameter and PIA Analysis.

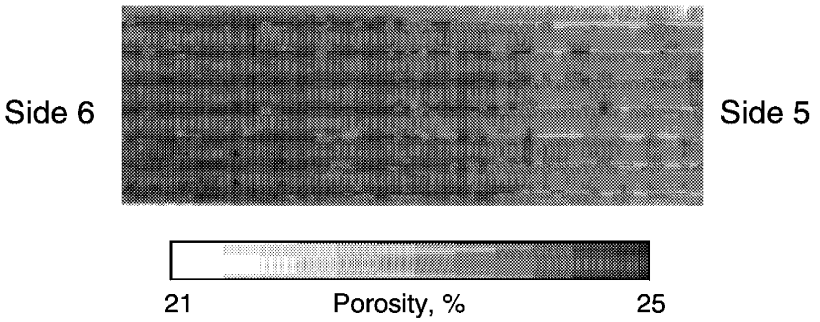

Figure 3–22 Porosity Map for CT-CF 12

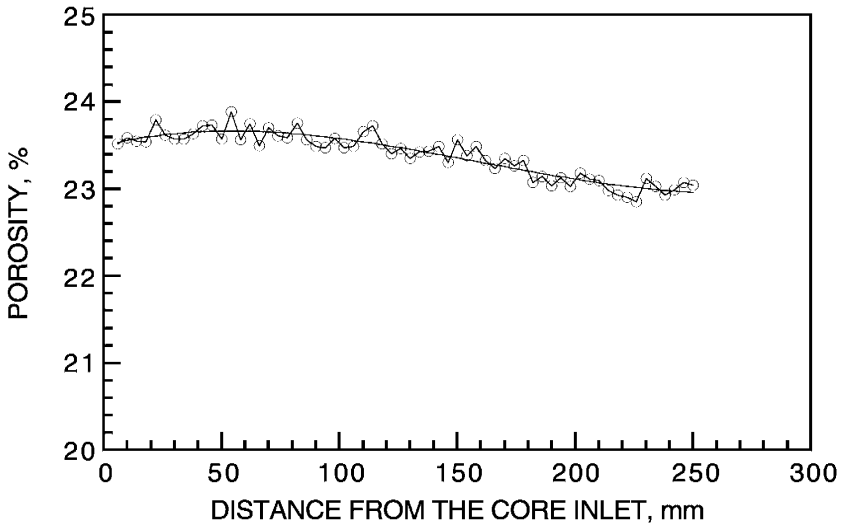

Figure 3–23 Average Porosity for CT-CF 12 from Side 6 to Side 5

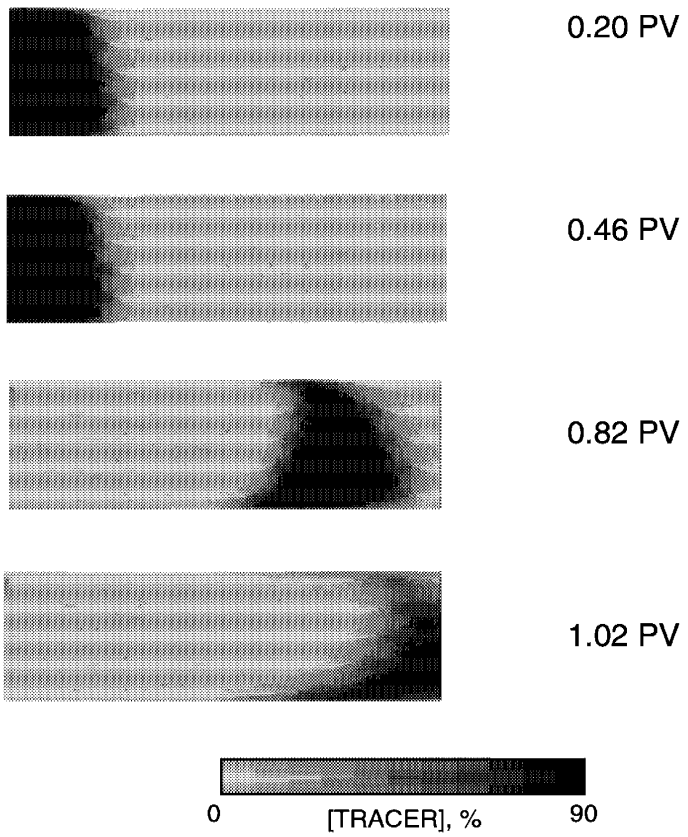

Figure 3–24 Profile of Brine Tracer Through Core CT-CF 12 for Various Amounts of Injected Fluid.

3.3.3 Description of the Chemical System

The surfactant system used in tests on sample CT-CF 12 consists of a petroleum sulfonate, Petronate-L (formally known as TRS 10-410) and a cosurfactant alcohol, IPA. The average molecular weight of the surfactant is 420 daltons. The chemicals form a three phase system with decane, with a microemulsion middle phase. Figure 3–25 shows a phase volume diagram for this system as a function of salinity. Reduction in temperature shifted the curves to slightly lower salinity. Addition of iododecane to decane also shifted the curves to lower salinity and increased the solubilization parameter for the mixed oil system. Optimal salinity for iododecane/decane system was approximately 1 wt% NaCl compared to approximately 1.2 wt% NaCl with no iododecane. Since the core was initially saturated with 1.7% NaCl and the injected aqueous chemical system contained 0.04% NaCl, as a result of dilution, the salinity of the system would pass through optimal salinity.

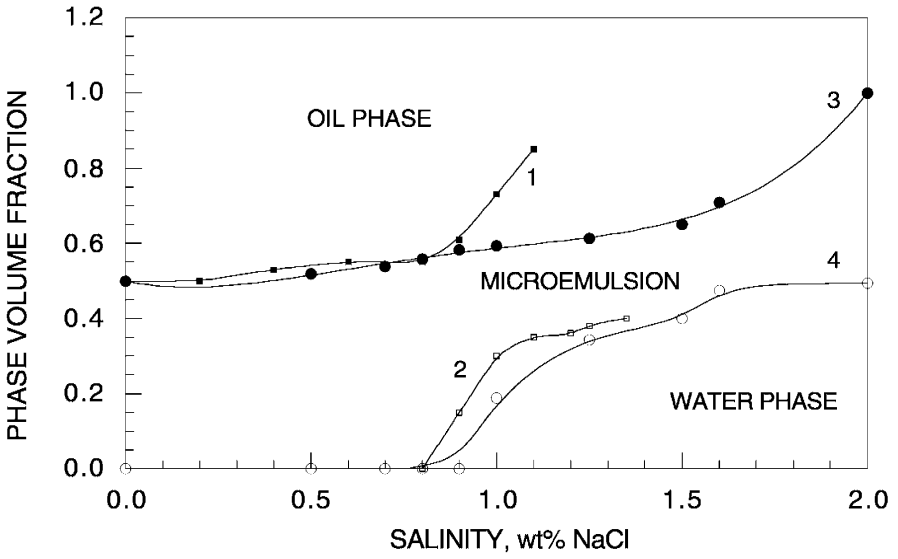

Figure 3–25 Phase Volume Fraction Diagram for Petroleum Sulfonate/Alcohol/Decane/ Brine System as a Function of Brine Salinity. Curves 1 and 2 are from Camilleri et al. (1987a) at 30°C, and curves 3 and 4 are for the system at 50°C.

The viscosity of the polymer slug as a function of shear rate is shown in Figure 3–26. The polymer acts as a non-Newtonian fluid; the apparent viscosity changes with a change in shear rate. The shear-rate dependence of the polymer viscosity can be modeled by Meter and Bird's (1964) equation:

$$\mu_p = \mu_\infty + \frac{\mu_p - \mu_\infty}{1 + (\gamma/\gamma_{1/2})^{P_\alpha - 1}} \tag{3–1}$$

where μ_p = polymer viscosity at a shear rate, cP

μ_∞ = polymer viscosity at infinite shear rate, cP

μ_o = polymer viscosity at 0 shear rate, cP

γ = shear rate, sec^{-1}

$\gamma_{1/2}$ = shear rate where viscosity is half its value between zero and infinite shear rate, sec^{-1}

P_α = shear rate dependence parameter for polymer

The parameters for a fit for the viscosity of 1,000 ppm polymer concentration are shown in Figure 3–26. A similar analysis for Xanthan polymer of different concentrations can be found in the literature (Camilleri et al. 1987b). Slight differences in the viscosity values determined in this

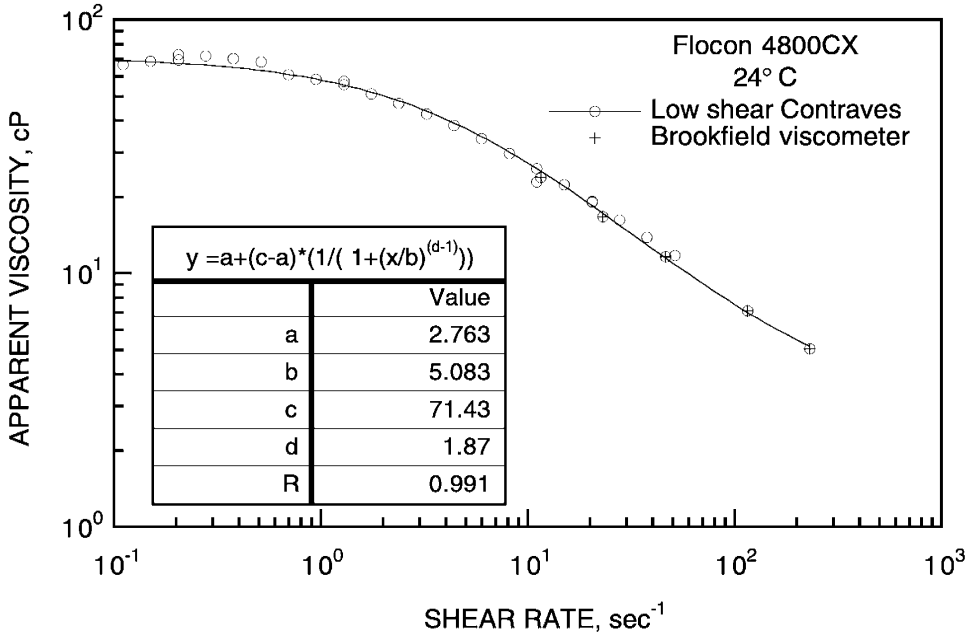

Figure 3–26 Viscosity as a Function of Shear Rate for 1,000 ppm Xanthan Biopolymer.

study with those published by Camilleri (from data in a MS thesis by Tsaur (1978)) can be attributed to the difference in salinity of the polymer solutions. Tsaur's solutions contained 1% NaCl; the polymer solution in this study contained 0.04% NaCl. The difference in viscosity at a shear rate of 5 sec^{-1} is in agreement with the data shown in Figure 14 of Camilleri paper (1987b) for Xanthan polymer viscosity as a function of salinity.

The similarity in solution properties of the chemicals used in this study and in Camilleri laboratory and simulation study indicate that results from these studies can be compared.

3.3.4 Oil Recovery and Analysis of Effluents

After completion of the tracer test, sample CT-CF 12 was flooded to residual water saturation using iododecane/decane. The average oil saturation at residual water saturation was 64%. The core was then waterflooded to residual oil saturation before starting the chemical IOR test. The average oil saturation after waterflood (S_{orw}) was 32%.

The tertiary oil recovery experiment was conducted after completion of the waterflood. Several times during the chemical flood, fluid injection was interrupted to determine the oil saturation distribution in the core (see Table 3–4). Effluent samples were collected using a fraction collector and analyzed for oil production, surfactant production, and effluent viscosity. Figure 3–27 shows

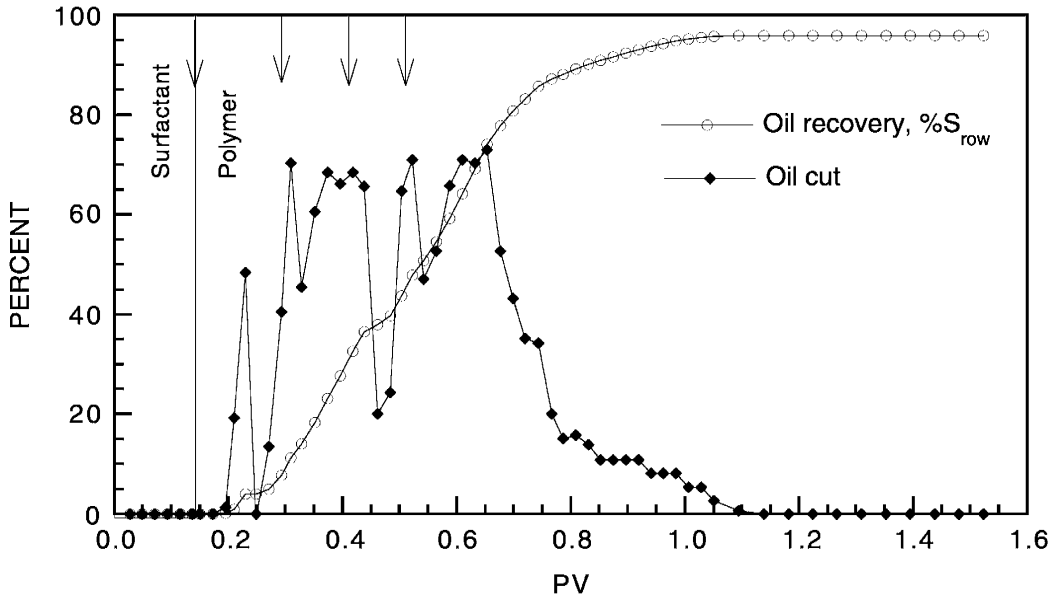

Figure 3–27 Cumulative Oil Production and Oil Cut for CT-CF 12. Arrows indicate when fluid injection was stopped to allow determination of the oil saturation distribution using CT-imaging.

the oil cut and cumulative oil production (as a percentage of S_{orw}) as a function of injected fluid PV. Oil broke through at 0.19 PV. High oil cuts started to decline after approximately 0.7 PV injected. Camilleri's test showed oil breakthrough at 0.17 PV and reduced oil cuts after 0.7 PV.

Fluid injection was interrupted several times to obtain CT images of the oil saturation distributions. Each interruption in flow resulted in a reduction in the oil cut as the fluid flow and pressure differential across the core was reestablished. Except for these interruptions, oil cuts were consistently above 60%. Oil recovery was 96% of the oil in place after waterflood.

Core effluent was analyzed for surfactant and for polymer viscosity. Figure 3–28 shows the relative surfactant and polymer production curves and the average pressure drop across the core.

Surfactant concentrations in the oil phase and water phase were not measured separately. Instead, the surfactant was extracted into the water phase by addition of IPA and analyzed as total surfactant produced during the flood. Surfactant was first detected after total injection reached 0.7 PV. The surfactant production curve peaked at approximately 0.85 PV to 1.0 PV and thereafter slowly declined. No surfactant was produced beyond 1.6 PV. Approximately 90% of the injected surfactant was detected in the effluent. These results compared with the surfactant production shown Figures 8 and 9 of the paper by Callimeri et al. (1987a). In that experiment, surfactant concentrations in the oil phase and water phase were measured separately. Surfactant

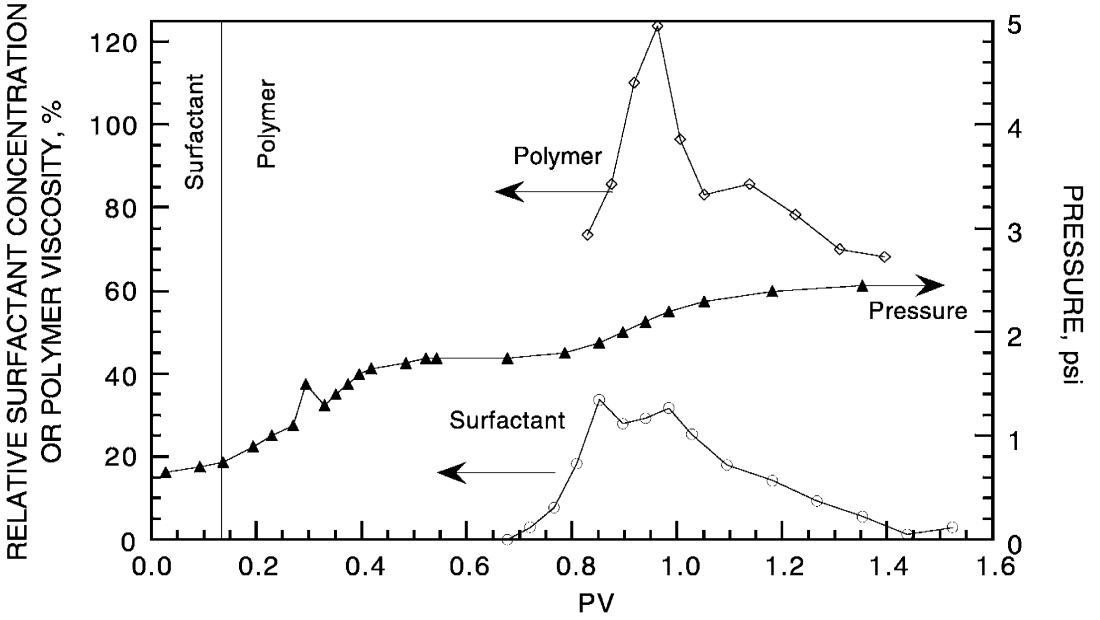

Figure 3–28 Pressure History and Production of Surfactant and Polymer During CT-CF 12.

was first detected at about 0.7 PV and peaked at 0.9 PV. This surfactant was produced in an oil or upper microemulsion phase (type III to type II+). Surfactant in the water phase (type II- microemulsion) broke through at 0.98 PV, declined steadily to 1.4 PV total volume injected. Thereafter, only trace amounts of surfactant were detected to 1.6 PV. Total recovery in this test was 100% of injected surfactant. Surfactant production in the water phase was attributed to the effectiveness of the salinity gradient and mobility control to redissolve absorbed surfactant and keep it mobilized behind the oil bank. Figure 3–29 shows a comparison of the surfactant production for the two tests.

Polymer viscosity peaked at approximately 0.95 PV fluid injected at a viscosity greater than the injected viscosity of the polymer slug. Camilleri also observed higher polymer concentration in the effluent than in the injected chemical slug. Polymer peaked at a concentration 30% higher than the injection concentration at 0.98 PV and then declined to a polymer concentration level equal to the injected polymer concentration.

The effluent analysis results indicated that, with only minor differences, the production characteristics of CT-CF 12 were comparable to those of Camilleri experiment.

Oil production, average pressure, and fluid analysis for CT-CF 12 is summarized in a Coreflood spreadsheet in Appendix A.

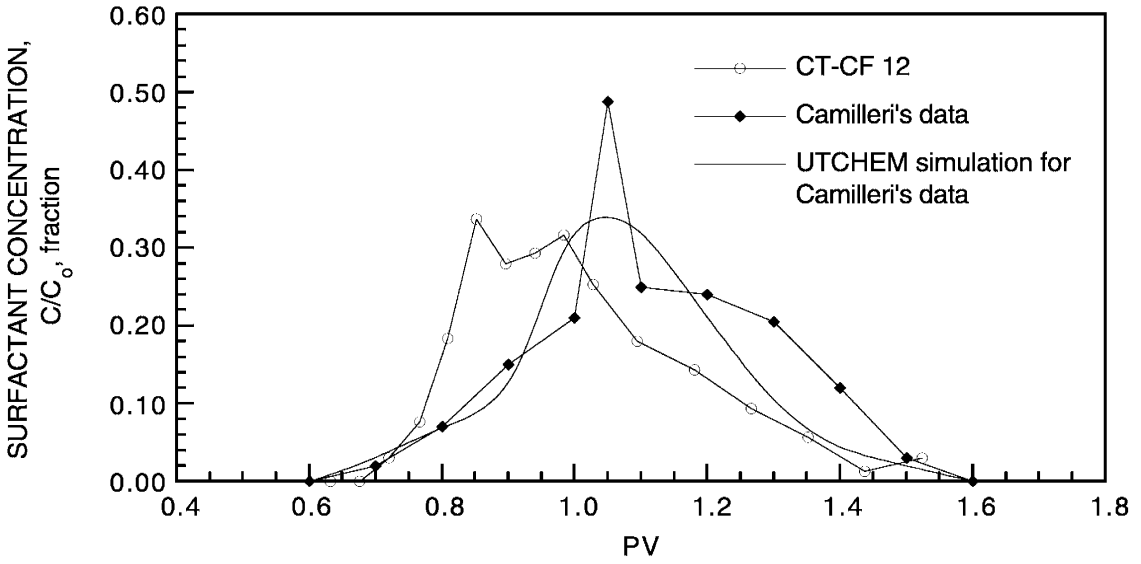

Figure 3–29 Comparison of Surfactant Production Curves for CT-CF 12 and for Camilleri's Results (1987a, see Figs. 8 and 9).

3.3.5 CT-Imaging and Simulation of Tracer

Simulation of tracer movement through the core was used to determine if the porosity/permeability distribution provided an adequate description for the core properties. Since the core appeared to be relatively uniform, the number of grid blocks in the porosity map was reduced from 140 x 140 x 63 to either 35 x 35 x 63 or 10 x 10 x 63 by averaging values of adjacent pixels. This reduced computation time.

The first simulation used UTCHEM to predict tracer movement through the core. The simulation, however, did not successfully describe the tracer profile. Severe numerical dispersion caused the tracer slug to spread over a much wider area of the core than was observed by the CT scanner. Figure 3–30 shows a comparison of the average profile shape after injection of 0.46 PV fluid. The simulation has not matched the tracer profile. Discussions are being held with personnel from the University of Texas to determine what parameters in the simulator need to be reviewed to minimize this problem.

While these discussions are in progress, two other simulators were used to simulate the tracer profiles as a function of fluid injected. These simulators were PC-GEL, a polymer profile modification simulator, and BOAST, a black oil simulator. Both of these simulators appeared to adequately describe the movement of tracer for CT-CF 12.

Figures 3–31 and 3–32 show the simulated tracer slug as it moved through the core for the 35 x 63 and 10 x 63 grids, respectively. The CT tracer images in Figure 3–24. The shape of the CT tracer slug showed a greater gravitational effect, caused by the density difference between tracer and in

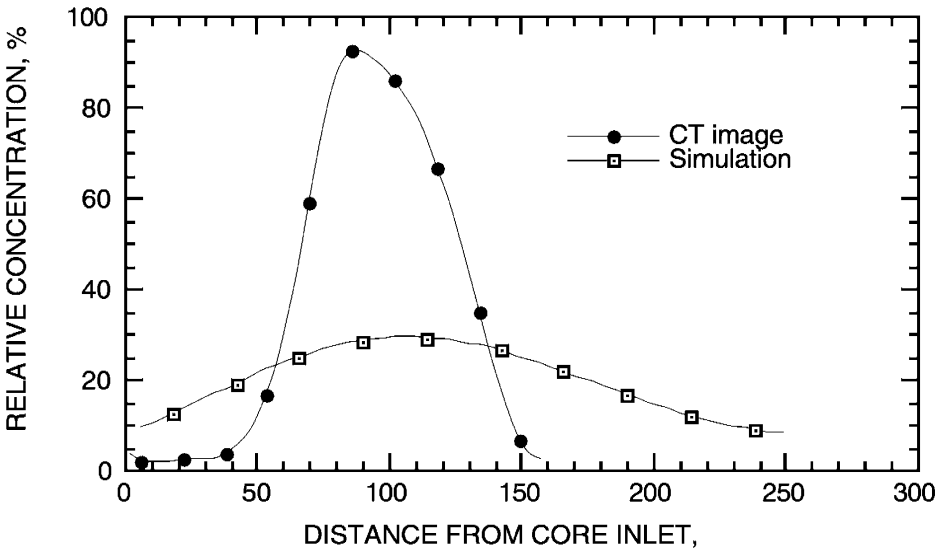

Figure 3–30 **Average Tracer Profile After 0.46 PV Injected for a Simulation Using UTCHEM as Compared With the Average Tracer CT Image Profile.**

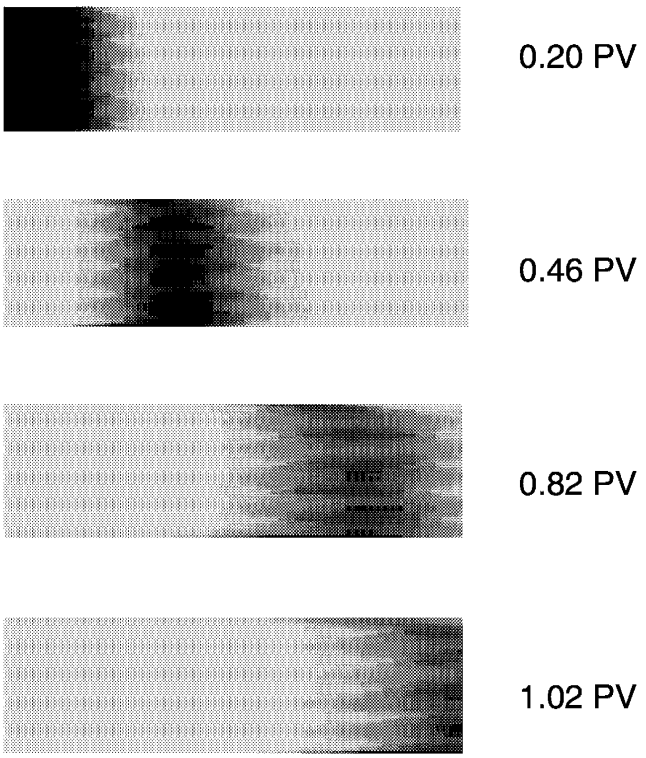

Figure 3–31 **Simulated Profile of Brine Tracer Through Core CT-CF 12 for Various Amounts of Injected Fluid Using a 35 x 63 Permeability/Porosity Grid with PC-GEL.**

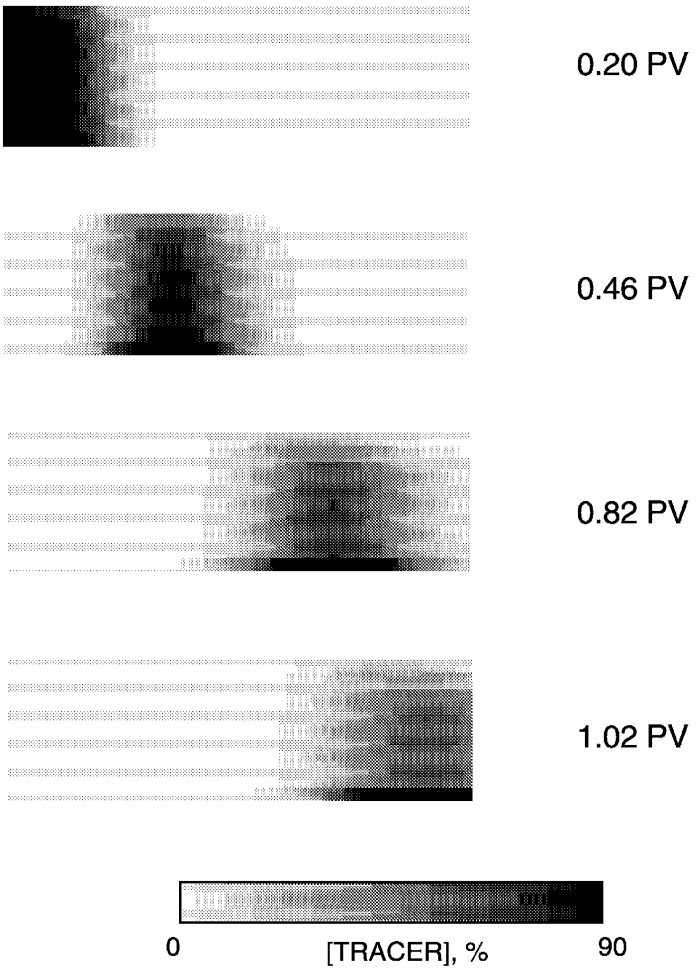

Figure 3–32 Simulated Profile of Brine Tracer Through Core CT-CF 12 Using a 10 x 62 Permeability/Porosity Grid with PC-GEL.

situ brine, than exhibited in the simulation profiles. Density differences that were used in the simulation are shown in Figure 3–33.

Figure 3–34 shows the tracer profile simulated using BOAST. In this case, equal horizontal and vertical permeabilities were selected. The density difference of the two brines caused the tracer to gravitate to the lower part of the core as the slug progressed through the core.

Figure 3–35 shows a comparison of the average tracer concentration value at the leading edge of the tracer slug from both the test the three separate simulations. BOAST reproduced the tracer front slightly better than either of the PC-GEL simulations.

BOAST will simulate a continuous tracer injection but is not set up to simulate a tracer slug injection. Two simulations, therefore, were run to simulate the front and back half of the slug. As a result, the total slug size in the simulation was smaller than the actual injected slug size. Figure 3–36 shows a comparison of the average tracer concentration as a function of position in the core

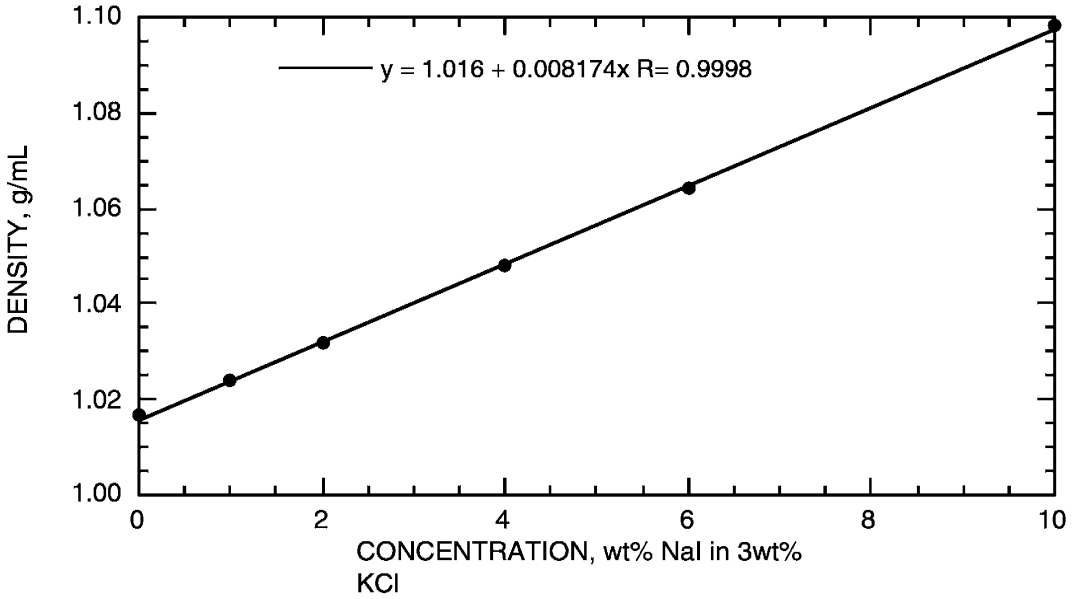

Figure 3–33 Density of Sodium Iodide in 3 wt% Potassium Chloride.

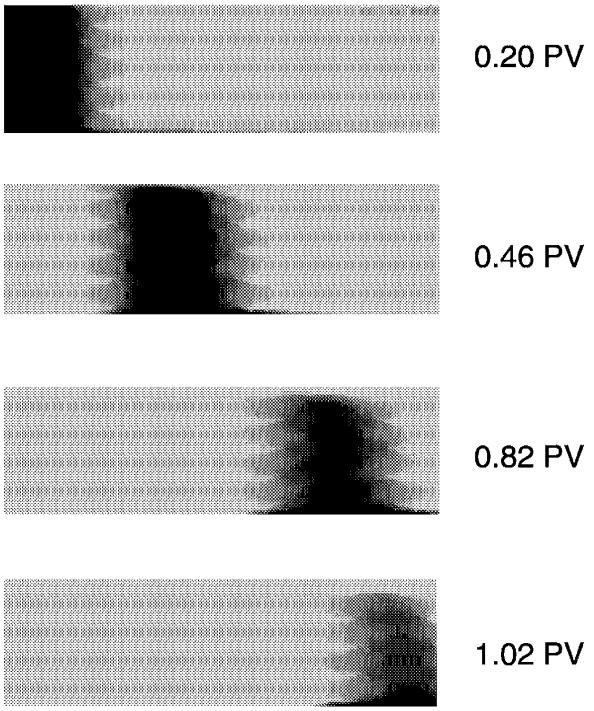

Figure 3–34 Simulation of CT-CF 12 Tracer Using BOAST.

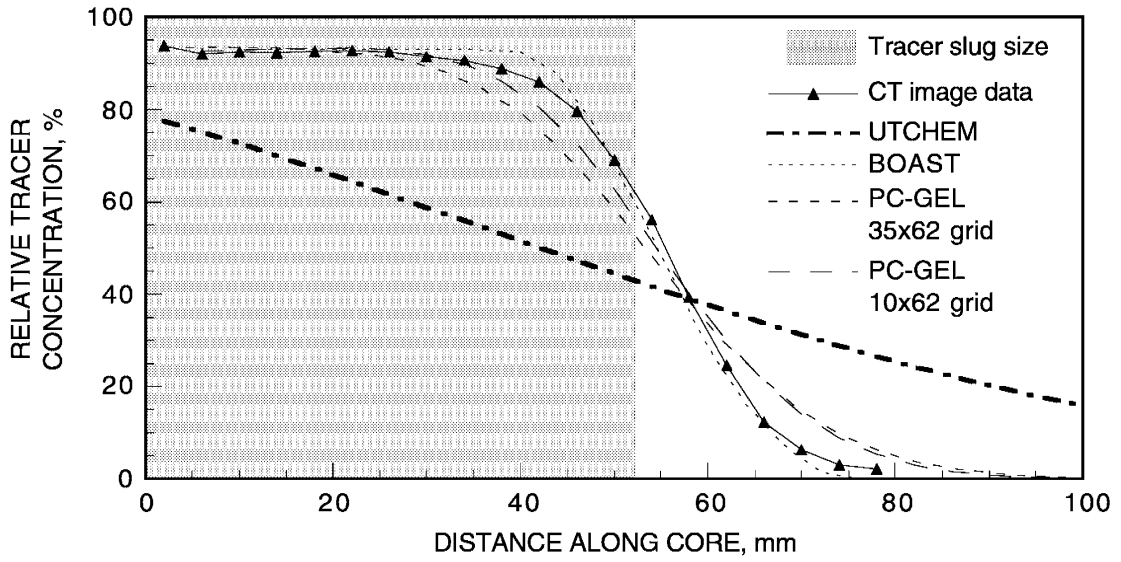

Figure 3–35 Comparison of the Tracer Fluid Fronts from CT Data and Simulations for 0.20 PV Fluid Injected.

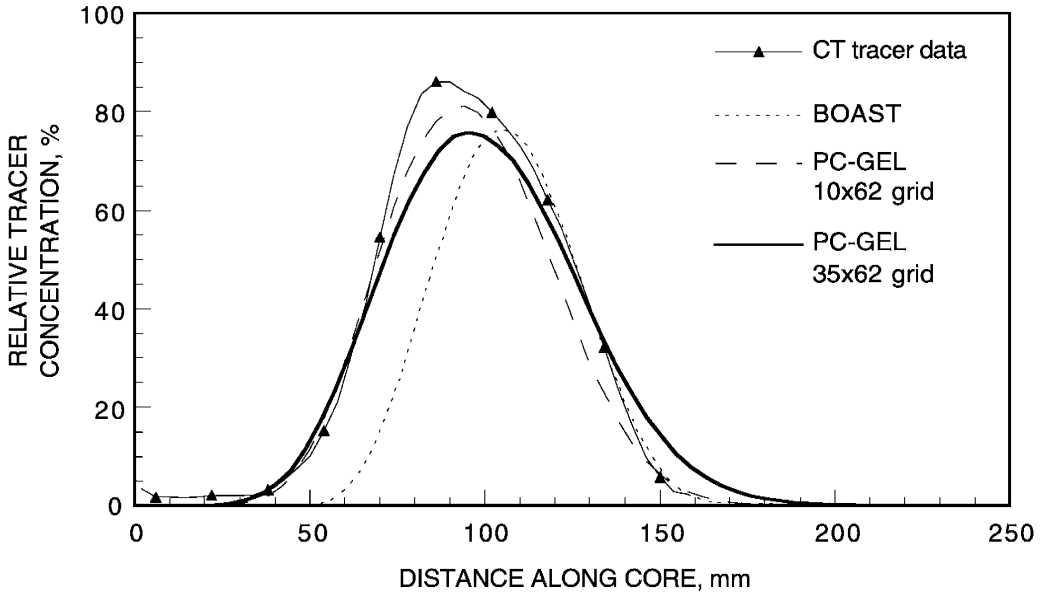

Figure 3–36 Comparison of the Tracer Fluid Fronts from CT Data and Simulations for 0.20 PV Fluid Injected.

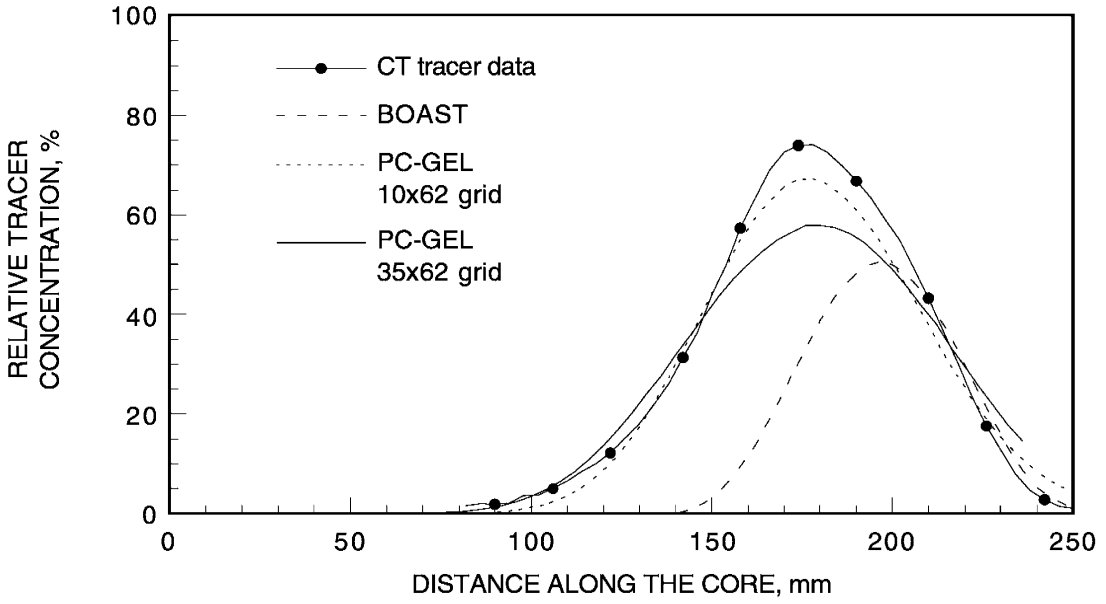

Figure 3–37 Comparison of the Tracer Fluid Front from CT Data and Simulations for 0.82 PV Fluid Injected.

after injection of 0.46 PV. All the simulations gave a reasonable comparison with the actual average tracer curve, although more numerical dispersion can be seen in the PC-GEL 35x63 simulation than in either of the other simulations. BOAST most closely modeled the tracer front. The small size of the BOAST slug was evident, however, in Figure 3–36. Figure 3–37 shows a similar comparison for the tracer profiles after injection of 0.82 PV. Again, the small size of the BOAST tracer slug was evident, but the front of the profile tracked well with the observed tracer slug. Of the two PC-GEL simulations, the 10x62 grid most closely described the observed average tracer shape.

Although further simulation refinements could be made, the available permeability and porosity maps provided an adequate description of the core. Finer permeability and porosity maps would be required if cores contained significant heterogeneities. Further studies are necessary, however, to identify the problems encountered using UTCHEM for tracer simulation.

3.3.6 CT-Imaging and Simulation of Chemical Flood

Figure 3–38 shows the CT images and Figure 3–39 shows the average oil saturations along the core after oil flood and waterflood, respectively. Figure 3–40 shows both the average oil saturations along the core and the corresponding CT images taken after injection of surfactant and different amounts of the polymer slug. These images represent a vertical slice down the middle of the core, not the average of each cross section. If all the vertical slices were averaged, however, the composite image of the saturation is nearly identical to that of the single vertical

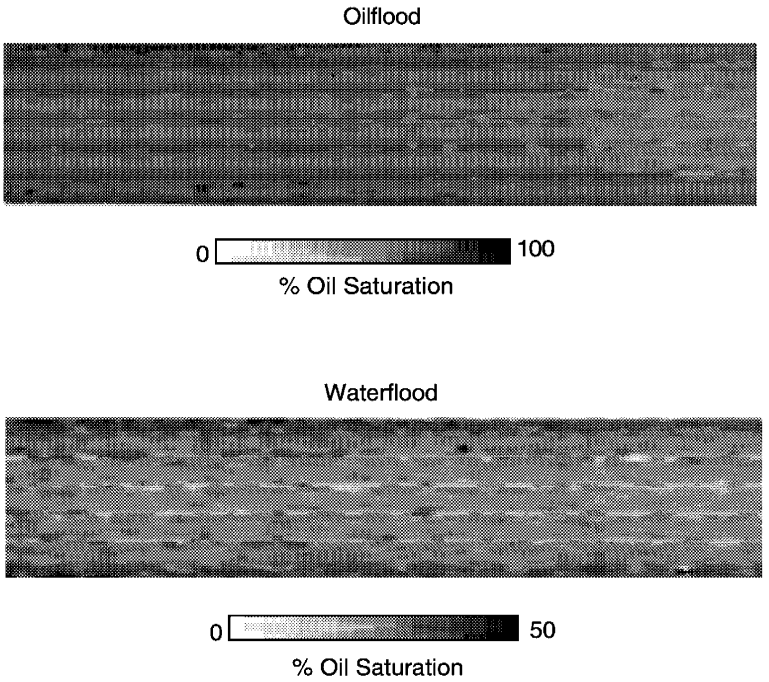

Figure 3–38 **CT Images of Oil Saturation Distributions After Oil Flood and Waterflood for CT-CF 12.**

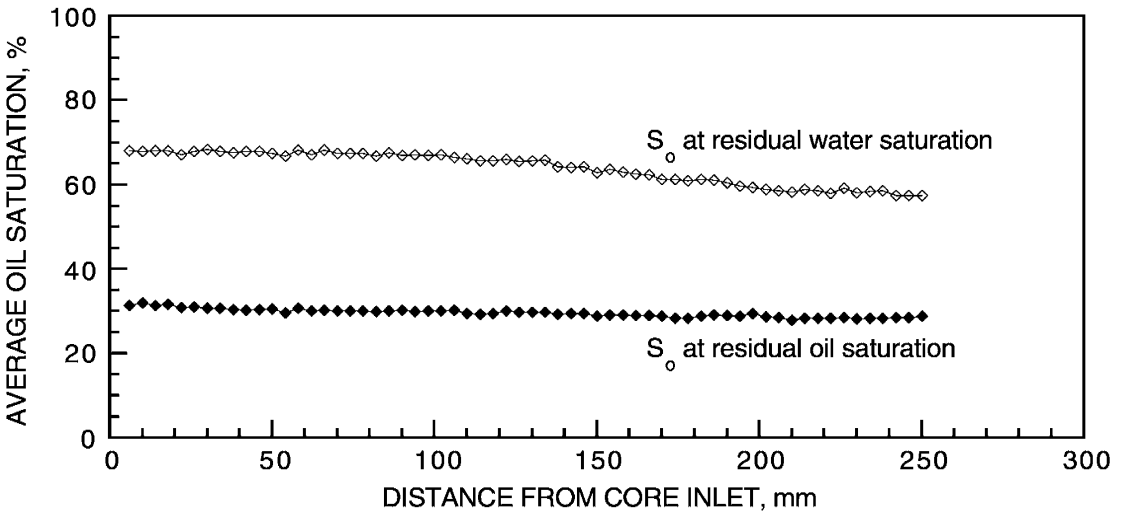

Figure 3–39 **Average Oil Saturation Along the Core After Oil Flood and for Test CT-CF 12 Waterflood.**

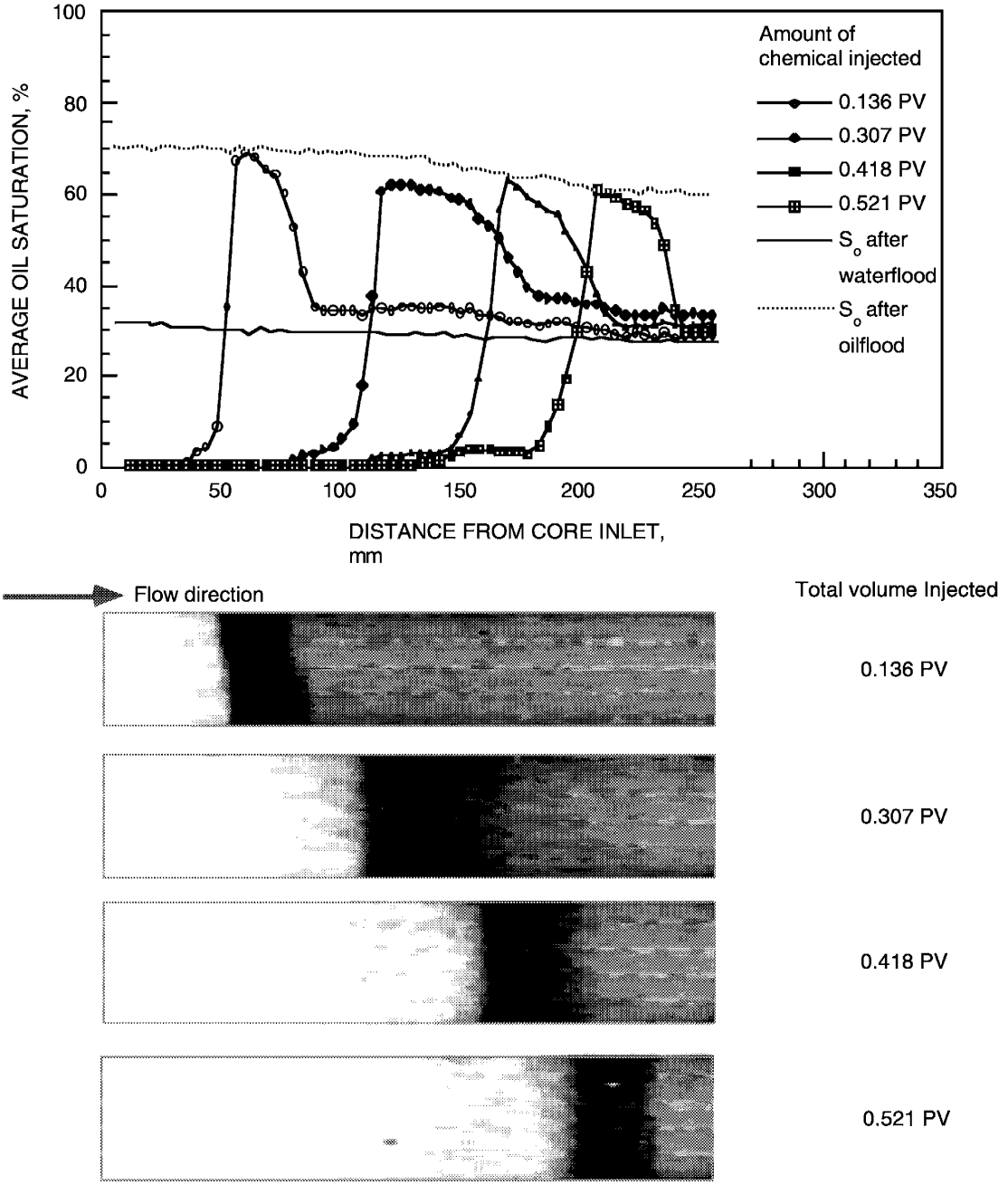

Figure 3–40 **Oil Saturation Distribution During CT-CF 12 Chemical Flood. The first image is after injection of the surfactant slug. The next three images are after injection of different amounts of the polymer mobility control slug.**

slice. Figure 3–41 shows the comparison of the single and averaged vertical slices at the end of surfactant injection. The position and shape of the oil bank are nearly identical, indicating uniform movement of the oil front.

The chemical slug produced a well defined oil bank that moved uniformly through the core. Essentially all of the oil was mobilized by the injected chemical. Movement of the oil bank indicates that the mobility control polymer retained its effectiveness throughout the test. As can be seen in Figure 3–40, the maximum oil saturation in the oil bank during the chemical flood reached the same value as the oil saturation measured at the end of the oil flood.

UTCHEM simulator input data were reviewed for the chemical IOR experiment. The input parameters and values used by the University of Texas researchers are listed in a Appendix B. Because of the problems with the tracer simulation, the simulation of test CT-CF 12 has not been completed at NIPER. Results of the comparable simulation conducted at the University of Texas were published in detail (Camilleri et al. 1987a). Their results will be used to discuss the oil saturation, as well as the surfactant and polymer production observed during the CT-CF 12 experiment.

Figure 3–42 shows a comparison of a simulated oil front after injection of 0.5 PV of fluid (as shown in Figure 11 of Camilleri's report) with the actual oil saturation distribution in test CT-CF 12 after injection of 0.52 PV. The simulation did not predict the formation of the oil bank. Furthermore, the position of the oil bank in the CT-CF 12 test was much closer to the core exit than expected. Although 52% of the core volume has been injected, approximately 77% of the core volume (V^1) has been swept of oil. Table 3-5 summarizes fluid volumes at this stage of the experiment. CT saturation values and material balance calculations indicated that over 42.8% of the original volume occupied by brine in V^1 has not been replaced by injected fluids while over

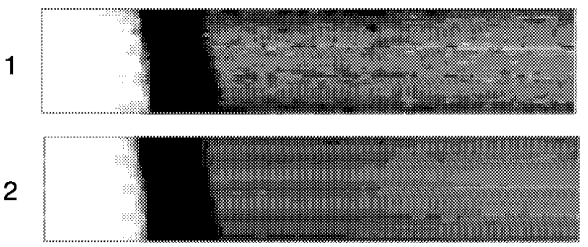

Figure 3–41 Comparison of the Oil Saturation Distribution After Surfactant Slug Injection of a Single Slice (1), One Pixel Wide, Down the Middle of the Core With the Average Oil Saturation for 140 Pixels (2). The similarity in the two images indicates that the oil front is moving uniformly through the core.

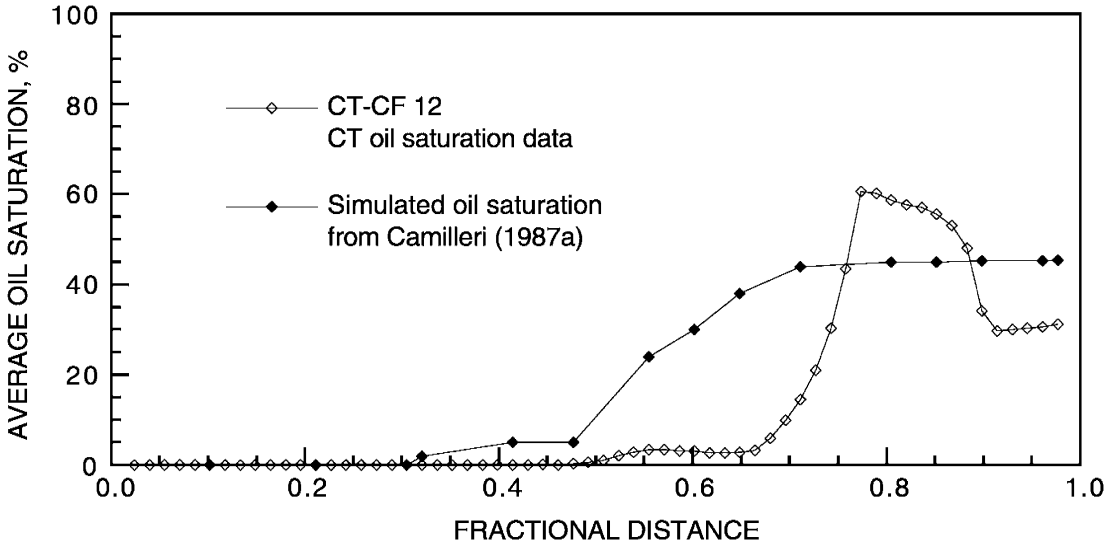

Figure 3–42 Comparison of the CT oil Saturation Distribution After Injection of 0.52 PV With the Simulated Oil Saturation Distribution Shown in Figure 11 of Camilleri's Paper.

Table 3–5 Summary of Initial Fluid Volumes and Fluid Volumes After Injection of 0.52 PV Surfactant and Polymer Slugs

#		Total volume, mL	Oil volume, mL	Aqueous volume, mL
1	Initial total PV	168	53.7	114.3
2	Volume (V^1) of core swept of oil after injection of 0.52 PV chemical slug	129		
3	Initial fluid composition of V^1		41.5	87.5
4	Initial fluids in remaining core (1-V^1) (#1-#2 or #1-#3)	39	12.2	27
5	Fluids produced after injection of 0.52 PV chemical slug	88	25.7	62.3
6	Oil moved from V^1 but not yet produced		12.3	
7	Total fluids displaced from V^1		38	50
8	Fluid volumes from V^1 that have not moved after injection of 0.52 PV chemical (#3-#7)		3.5	37.5

92% of V^1 occupied by oil has been mobilized by the chemical injection. (The brine volume not swept by chemical was approximately 30% of V^1.)

Because of their large hydrodynamic size, polymer molecules are known to be excluded from the smaller pores. In addition, polymer adsorption on the rock surface may reduce pore sizes, increasing the pore volume inaccessible to polymers. Previous researchers have determined that a relationship exists between inaccessible pore volume and the irreducible water saturation found in the presence of oil (Dawson and Lautz, 1972). For CT-CF 12, the water saturation at the end of the waterflood was approximately 35%. The excluded volume was approximately 30% of V^1. This compares with the connate water saturation for this core.

Capillary forces can cause water to enter and displace oil from pores inaccessible to polymer. As a result, polymer may concentrate in the remaining water. Increased polymer concentration was observed for both CT-CF 12 (see Fig. 3–28) and Camilleri's test (see Fig 12 in reference 1987a). In a chemical flood, the surfactant can change the capillary forces and further enhance the ability of water to displace oil from pores inaccessible to polymer. UTCHEM has the capability of adjusting both polymer and surfactant inaccessible pore volume. Some additional adjustments may be necessary to model the buildup of oil in the oil bank that is actually observed using CT imaging.

The ability to observe and quantify the oil recovery mechanisms using CT imaging allow improvements in the experimental methods to evaluate and design chemical flooding formulations. CT-CF 12 provides a very clear picture of an effective chemical system and resulting oil production. Well defined CT experiments in different types of porous media (wettability, pore size, heterogeneity) can be compared to this very effective oil recovery experiment.

4.0 SUMMARY AND CONCLUSIONS

Screening studies were conducted on a select surfactant system, containing a nonionic and an anionic component. The effects of different variables on the oil recovery were evaluated. Conventional and CT-monitored experiments were conducted to screen the chemical formulation. The parameters evaluated included: chemical injection strategy, chemical slug size, core effective permeability, and polymer concentration.

Chemical slug injection were evaluated in different permeability Berea sandstone core for different chemical injection strategies. All comparisons showed that the injection of middle-phase chemical slugs yielded better oil displacement compared to the straight chemical injection. Oil recovery heavily favored application in high permeability cores. Recovery in the low permeability cores was severely restricted by poor sweep. CT-monitored experiments indicated the presence of relatively high oil saturation "streaks" in the low permeability regions of the core.

Optimal chemical slug size was determined for a mixed surfactant chemical system. The results indicated an optimal chemical slug size of about 25% PV for both middle-phase and nonequilibrated chemical slug injection. Although oil saturations further reduced by using chemical slug volumes greater than 30%, treatment cost is increased significantly.

Efforts to improve the sweep efficiency of the chemical system were undertaken, particularly for the case of the nonequilibrated chemical slug injection. Although the surfactant slug was effective in displacing (banking) oil in the contacted areas, it "stalled" during the polymer and brine injections. Experiments were conducted to determine the effect of polymer loading on displacement behavior. These experiments provided an indication of required optimal polymer concentration loading. The results of these experiments were compared with experiments using a salinity gradient approach, with the polymer slug formulated in fresh water, followed by a brine slug.

Results of oil recovery experiments using 500 and 1,000 ppm polymer concentrations were relatively poor. Experiments using 2,000 and 3,000 ppm polymer concentrations produced much more oil; higher polymer loadings delayed but sustained oil production during the polymer injection cycle. The results from the 1,500 ppm polymer concentration experiment yielded only a slight improvement over the two lower concentration experiments. These experiments support the observation that a lower threshold value for polymer loading (minimum mobility requirement) is needed to achieve improved displacement.

These results were compared with the results from salinity gradient experiments using 1,000 ppm biopolymer for mobility control. The salinity gradient approach ensures optimal conditions for oil solubilization and mobilization during chemical injection and helps to reduce surfactant loss by adsorption and trapping. The final oil saturations from the salinity gradient experiments

were much better than saturations obtained at the lower polymer concentration experiments. The overall results support the following trend:

500 ppm ≤ 1,000 ppm < 1,500 ppm < 2,000 ppm < salinity gradient @ 1,000 ppm < 3,000 ppm

Application of a salinity gradient in the polymer slug with the straight chemical slug injection scheme is the preferred chemical oil displacement method for the mixed surfactant system used in this study.

CT imaging of oil saturation during a chemical IOR oil recovery experiment was conducted to determine the oil saturation distribution during chemical injection. The chemical system selected has been studied extensively. Total oil recovery and production of polymer and surfactant agreed with previously reported data. Simulation of the oil front after injection of 0.5 PV chemical was very different from the observed CT oil saturation. The simulation did not show the buildup of an the oil bank. During the chemical flood, polymer did not invade a significant percentage of the core pore volume (approximately 30% PV).

Permeability and porosity characteristics for the test sample were determined using a minipermeameter, CT image, and tracer tests. A porosity and permeability map was constructed for use in simulation. Two simulators, BOAST and PC-GEL provided reasonable tracer simulation results using these permeability and porosity values. UTCHEM did not simulate the tracer profile; further evaluation is required to determine the nature of the problem.

The ability to observe and quantify the oil recovery mechanisms using CT imaging can improve experimental methods to evaluate and design chemical flooding. Test CT-CF 12 provides a very clear picture of an effective chemical system and resulting oil production. Well defined CT experiments in different types of porous media (wettability, pore size, heterogeneity) using chemical systems with different degrees of effectiveness can be compared to this very effective oil recovery experiment.

5.0 REFERENCES

Camilleri, D., A. Fil, G. A. Pope, B. A. Rouse, and K Sepehrnoori. 1987a. Comparison of an Improved Compositional Micellar/Polymer Simulator with Laboratory Corefloods. *SPE Reservoir Engineering.* November, p. 441-451.

Camilleri, D., S. Engelsen, L. W. Lake, E. C. Lin, T. Ohno, G. Pope, and K. Sepehrnoori. 1987b. Description of an Improved Compositional Micellar/Polymer Simulator. *SPE Reservoir Engineering,* November, p. 427-432.

Chang, M. M., P. Sarathi, R. L. Heemstra, A. M. Cheng, and J. F. Pautz. 1991. *User's Guide and Documentation Manual for "BOAST-VHS for the PC,* Topical Report NIPER-542, July.

Dawson, R. and R. B. Lantz. 1972. Inaccessible Pore Volume in Polymer Flooding. SPEJ, October, p. 448-452.

Delshad, M. 1990. Trapping of Micellar Fluids in Berea Sandstone. Ph.D. Dissertation, University of Texas at Austin, August

Delshad, M., M. Delshad, D. Bhuyan, G. A. Pope, and L. W. Lake. 1986. Effect of Capillary Number on the Residual Saturation of a Three-Phase Micellar Solution. SPE/DOE Paper 14911 presented at the Fifth Symposium on Enhanced Oil Recovery, April 20-23, Tulsa, OK.

Gall, B. L. 1992. *CT Imaging of Enhanced Oil Recovery Experiments.* Department of Energy Report No. NIPER-611, December.

Gao, H. W. and M. M. Chang. 1990. *A Three-Dimensional, Three-Phase Simulator for Permeability Modification Treatments Using Gelled Polymers,* Department of Energy Report No. NIPER-388, March.

Llave, F. M. and D. K. Olsen. 1988. *Development of an Automated System for Phase Inversion Temperature Measurements.* Department of Energy Report No. NIPER-318, June.

Llave, F. M., T. R. French, and P. Lorenz. 1992a. *Evaluation of Mixed Surfactants for Improved Chemical Flooding.* Department of Energy Report - NIPER-631, November.

Llave, F. M., B. L. Gall, and L. A. Noll. 1990. *Mixed Surfactant Systems for Enhanced Oil Recovery.* Department of Energy Report No. NIPER-497, December.

Llave, F. M., B. L. Gall, T. R. French, L. A. Noll, and S. A. Munden. 1992b. *Phase Behavior and Oil Recovery Investigations Using Mixed and Alkaline-Enhanced Surfactant Systems.* Department of Energy Report No. NIPER-567, March.

Llave, F.M., B. L. Gall, H. W. Gao, L. J. Scott, and I. M. Cook. 1994. *Chemical Systems for Improved Oil Recovery: Phase Behavior, Oil Recovery, and Mobility Control Studies.* Department of Energy Report No. NIPER/BDM-0074, September.

Llave, F. M. B. L. Gall, P. Lorenz, I. M. Cook, and L.J. Scott. 1993. *Screening of Mixed Surfactant Systems: Phase behavior Studies and CT Imaging of Surfactant-Enhanced Oil Recovery Experiments.* Department of Energy Report - NIPER-710, September.

Lorenz, P. B. and S. Brock. 1987. *Surfactant and Cosurfactant Properties of Mixed and Polysulfonated Surfactant by Phase Volume Measurements.* Department of Energy Report No. NIPER-256, October.

Meter, D. M. and R. B. Bird. 1964. Tube Flow of Non-Newtonian Polymer Solutions: Part 1, Laminar Flow and Rheological Models. *AIChE J*, November, p. 878-881.

Pope, G. A. and R. C. Nelson. 1978. A Chemical Flooding Compositional Simulator. *SPEJ* (October, 1978), p. 357-368.

Private communication with Witco representative. 1994.

Prouvost, L., G. A. Pope, and B. A. Rouse. 1985. Microemulsion Phase Behavior: A Thermodynamic Modeling of the Phase Partitioning of Amphiphilic Species. *SPEJ* (October 1985) p. 693.

Prouvost, L., T. Satoh, K. Sepehrnoori, and G. A. Pope. 1984. A New Micellar Phase-Behavior Model for Simulating Systems With Up to Three Amphiphilic Species. SPE Paper 13031 presented at the 59th Annual Technical Conference, Sept. 16-19, Houston, TX.

Satoh, T. 1984. Treatment of Phase Behavior and Associated Properties Used in a Micellar-Polymer Flood Simulator. Master's Thesis, University of Texas at Austin, August.

Tomutsa, L. D., D. Doughty, S. Mahmood, A. Brinkmeyer, and M. Madden. 1990. *Imaging Techniques Applied to the Study of Fluids in Porous Media.* Dept. of Energy Report No. NIPER-485, August.

Tsaur, K. 1987. A Study of Polymer/Surfactant Interaction for Micellar/Polymer Flooding. Master's Thesis, University of Texas at Austin.

APPENDIX A

CT-CF 12 coreflood spreadsheet summarizes core properties and fluid production during the chemical flooding experiment conducted to determine oil saturation distributions during chemical injection.

Table A–1 NIPER Coreflood Report—CT-CF 12

NOTEBOOK: B-025 **OPERATOR:** ALAN MILLER
CORE NUMBER: CT-CF12 **DATE:** 12/12/94
CORE TYPE: BEREA **CLIENT:** DOE

CORE DIMENSIONS

LENGTH(cm): 26.00 **AREA:** 27.83 **BULK VOLUME(cc):** 723.58

COREFLOOD SET-UP:

ENCAPSULATION: EPOXY **TEMP (°C):** 73.00
OVERBURDEN(psi): NONE **PRESSURE(psi):** 0.00

COREFLOOD FLUIDS

BRINE COMP: 1.7% NaCl
OIL: 80% Decane/20% Iododecane by weight
SURF(S). COMP: 2.98%Petronate-L, 3% IPA, 992ppm Flocon 4800CX in .037% NaCl
POLYMER: 1000 ppm Flocon 4800CX in .04% NaCl
TRACER: none

PURPOSE OF THE FLOOD:

Purpose 1 CT IMAGING
Purpose 2 GOOD OIL RECOVERY CASE
Purpose 3 HIGH PERMEABILITY CASE

ADDITIONAL NOTES:

surfactant slug density = 0.993
(dead volume not removed from total volume for purposes of

REPORT SECTION

PV (ml):	168.20	Sat. %		**POROSITY:**	23.25	Percent
INITIAL OIL SATN.(ml):	109.00	64.80	- - -	**PERMEABILITY:**	195.70	md
REM. OIL AFTER WATERFLOOD(ml):	53.70	31.93	55.30	**OIL TYPE:**		
REM. OIL AFTER CHEMICAL FLOOD (ml)	2.25	1.34	51.45	**OIL VISCOSITY:**	1.00	cP
RECOVERY EFFICIENCY (%):	95.81			**OIL DENSITY:**	0.8198	g/cc

TERTIARY RECOVERY

TUBE NO.	TOTAL (ml)	WATER VOLUME (ml)	OIL VOLUME (ml)	SUM of TOT. VOL. (ml)	SUM of OIL VOL (ml)	Res Oil Sat Socf (%PV)	Oil Rec % (%PV)	PV Injected	Oil/Wat Ratio	Oil Cut (%)	Comments	Surf, %	Viscosity cP at rpm 30	PRESSURE .122ML/MIN
0	0.00	0.00	0.00	0.00	0.00	31.93	0.00	0.0000						
1	4.60	4.60	0.00	4.60	0.00	31.93	0.00	0.0273	0.0000	0.00				0.65
2	3.50	3.50	0.00	8.10	0.00	31.93	0.00	0.0482	0.0000	0.00				
3	3.70	3.70	0.00	11.80	0.00	31.93	0.00	0.0702	0.0000	0.00				
4	3.70	3.70	0.00	15.50	0.00	31.93	0.00	0.0922	0.0000	0.00				0.7
5	3.70	3.70	0.00	19.20	0.00	31.93	0.00	0.1141	0.0000	0.00				
6	3.70	3.70	0.00	22.90	0.00	31.93	0.00	0.1361	0.0000	0.00				0.75
7	2.30	2.30	0.00	25.20	0.00	31.93	0.00	0.1498	0.0000	0.00	start poly			
8	3.70	3.70	0.00	28.90	0.00	31.93	0.00	0.1718	0.0000	0.00				
9	3.70	3.65	0.05	32.60	0.05	31.90	0.09	0.1938	0.0137	1.35				0.9

Table A–1 NIPER Coreflood Report—CT-CF 12

TUBE NO.	TOTAL (ml)	WATER VOLUME (ml)	OIL VOLUME (ml)	SUM of TOT. VOL. (ml)	SUM of OIL VOL (ml)	Res Oil Sat Socf (%PV)	Oil Rec % (%PV)	PV Injected	Oil/Wat Ratio	Oil Cut (%)	Comments	Surf, %	Viscosity, cP at rpm 30	PRESSURE .122ML/MIN
10	2.60	2.10	0.50	35.20	0.55	31.60	1.02	0.2093	0.2381	19.23				
11	3.30	1.70	1.60	38.50	2.15	30.65	4.00	0.2289	0.9412	48.48				1
12	3.30	3.30	0.00	41.80	2.15	30.65	4.00	0.2485	0.0000	0.00				
13	3.70	3.20	0.50	45.50	2.65	30.35	4.93	0.2705	0.1563	13.51				1.1
14	3.70	2.20	1.50	49.20	4.15	29.46	7.73	0.2925	0.6818	40.54				1.5
15	2.70	0.80	1.90	51.90	6.05	28.33	11.27	0.3086	2.3750	70.37				
16	3.30	1.80	1.50	55.20	7.55	27.44	14.06	0.3282	0.8333	45.45				1.3
17	3.80	1.50	2.30	59.00	9.85	26.07	18.34	0.3508	1.5333	60.53				1.4
18	3.80	1.20	2.60	62.80	12.45	24.52	23.18	0.3734	2.1667	68.42				1.5
19	3.70	1.25	2.45	66.50	14.90	23.07	27.75	0.3954	1.9600	66.22				1.6
20	3.80	1.20	2.60	70.30	17.50	21.52	32.59	0.4180	2.1667	68.42				1.65
21	3.20	1.10	2.10	73.50	19.60	20.27	36.50	0.4370	1.9091	65.63				
22	4.00	3.20	0.80	77.50	20.40	19.80	37.99	0.4608	0.2500	20.00				
23	3.70	2.80	0.90	81.20	21.30	19.26	39.66	0.4828	0.3214	24.32				1.7
24	3.40	1.20	2.20	84.60	23.50	17.95	43.76	0.5030	1.8333	64.71				
25	3.10	0.90	2.20	87.70	25.70	16.65	47.86	0.5214	2.4444	70.97				1.75
26	3.40	1.80	1.60	91.10	27.30	15.70	50.84	0.5416	0.8889	47.06				1.75
27	3.80	1.80	2.00	94.90	29.30	14.51	54.56	0.5642	1.1111	52.63				
28	3.80	1.30	2.50	98.70	31.80	13.02	59.22	0.5868	1.9231	65.79				
29	3.80	1.10	2.70	102.50	34.50	11.41	64.25	0.6094	2.4545	71.05				
30	3.70	1.10	2.60	106.20	37.10	9.87	69.09	0.6314	2.3636	70.27		0.00		
31	3.70	1.00	2.70	109.90	39.80	8.26	74.12	0.6534	2.7000	72.97				
32	3.80	1.80	2.00	113.70	41.80	7.07	77.84	0.6760	1.1111	52.63		0.00		1.75
33	3.70	2.10	1.60	117.40	43.40	6.12	80.82	0.6980	0.7619	43.24				
34	3.70	2.40	1.30	121.10	44.70	5.35	83.24	0.7200	0.5417	35.14		0.09		
35	3.80	2.50	1.30	124.90	46.00	4.58	85.66	0.7426	0.5200	34.21				
36	4.00	3.20	0.80	128.90	46.80	4.10	87.15	0.7663	0.2500	20.00		0.23		
37	3.30	2.80	0.50	132.20	47.30	3.80	88.08	0.7860	0.1786	15.15	emulsion			1.8
38	3.80	3.20	0.60	136.00	47.90	3.45	89.20	0.8086	0.1875	15.79	emulsion	0.55		
39	3.60	3.10	0.50	139.60	48.40	3.15	90.13	0.8300	0.1613	13.89	emulsion			
40	3.70	3.30	0.40	143.30	48.80	2.91	90.88	0.8520	0.1212	10.81	emulsion	1.01		1.9
41	3.70	3.30	0.40	147.00	49.20	2.68	91.62	0.8740	0.1212	10.81	emulsion		5.66	
42	3.70	3.30	0.40	150.70	49.60	2.44	92.36	0.8960	0.1212	10.81	emulsion	0.84		2
43	3.70	3.30	0.40	154.40	50.00	2.20	93.11	0.9180	0.1212	10.81	emulsion		6.60	
44	3.70	3.40	0.30	158.10	50.30	2.02	93.67	0.9400	0.0882	8.11		0.88		2.1
45	3.70	3.40	0.30	161.80	50.60	1.84	94.23	0.9620	0.0882	8.11			8.48	
46	3.70	3.40	0.30	165.50	50.90	1.66	94.79	0.9839	0.0882	8.11		0.95		2.2
47	3.70	3.50	0.20	169.20	51.10	1.55	95.16	1.0059	0.0571	5.41			9.54	
48	3.70	3.50	0.20	172.90	51.30	1.43	95.53	1.0279	0.0571	5.41		0.76		
49	3.70	3.60	0.10	176.60	51.40	1.37	95.72	1.0499	0.0278	2.70			7.44	2.3
50	7.40	7.35	0.05	184.00	51.45	1.34	95.81	1.0939	0.0068	0.68		0.54		
51	7.40	7.40	0.00	191.40	51.45	1.34	95.81	1.1379	0.0000	0.00			6.40	
52	7.25	7.25	0.00	198.65	51.45	1.34	95.81	1.1810	0.0000	0.00		0.43		2.4
53	7.20	7.20	0.00	205.85	51.45	1.34	95.81	1.2238	0.0000	0.00			6.60	
54	7.05	7.05	0.00	212.90	51.45	1.34	95.81	1.2658	0.0000	0.00		0.28		
55	7.30	7.30	0.00	220.20	51.45	1.34	95.81	1.3092	0.0000	0.00			6.04	
56	7.20	7.20	0.00	227.40	51.45	1.34	95.81	1.3520	0.0000	0.00		0.17		2.45
57	7.15	7.15	0.00	234.55	51.45	1.34	95.81	1.3945	0.0000	0.00			5.39	
58	7.15	7.15	0.00	241.70	51.45	1.34	95.81	1.4370	0.0000	0.00		0.04		
59	7.20	7.20	0.00	248.90	51.45	1.34	95.81	1.4798	0.0000	0.00			5.25	
60	7.30	7.30	0.00	256.20	51.45	1.34	95.81	1.5232	0.0000	0.00	cloudy	0.09		

APPENDIX B

In preparation for simulation of the chemical flood, the input requirements for data needed to simulate a chemical IOR experiment using UTCHEM simulator were reviewed. Table B–1 shows the physical properties (phase behavior parameters at zero, one and twice optimal salinity, alcohol partitioning parameters, interfacial tension parameters, capillary-saturation curve parameters, relative permeability parameters of the oil, aqueous, and microemulsion phases of the mixture, and viscosity parameters for a biopolymer) of an chemical slug - oil mixture that consisted of 1.5 vol% active TRS 10-410, 1.5 vol% IBA, 47 vol% brine and 50 vol% n-decane (oil:water ratio = 1:1). This mixture had been studied extensively at the University of Texas (Camilleri et al. 1987a; Delshad, 1990; Delshad et al. 1986, Prouvost et al. 1984 and 1985; Satoh, 1984).

Table B–1 Input Parameters for Simulation of a Surfactant/Polymer Coreflood Using UTCHEM

Definition	Parameter	Value	Units
Phase behavior parameters			
Oil conc. at plait point in type II(+) region	C2PLC	0.	volume fraction
Oil conc. at plait point in type II(-) region	C2PRC	1.	volume fraction
Critical micellar conc.	EPSME	0.0001	volume fraction
Slope for max. height of binodal curve vs. fraction of IBA associated with surfactant at zero salinity	HBNS70	0.131	volume fraction
Intercept of max. height of binodal curve at zero fraction of IBA associated with surfactant at zero salinity	HBNC70	0.1	volume fraction
Slope for max. height of binodal curve vs. fraction of IBA associated with surfactant at optimal salinity	HBNS71	0.191	volume fraction
Intercept of max. height of binodal curve at zero fraction of IBA associated with surfactant at optimal salinity	HBNC71	0.026	volume fraction
Slope for max. height of binodal curve vs. fraction of IBA associated with surfactant at twice optimal salinity	HBNS72	0.363	volume fraction
Intercept of max. height of binodal curve at zero fraction of IBA associated with surfactant at twice optimal salinity	HBNC72	0.028	volume fraction
Lower effective salinity limit for type III phase	CSEL7	0.177	meq/mL
Upper effective salinity limit for type III phase	CSEU7	0.344	meq/mL
The effective salinity slope parameter for IBA	BETA7	-2.0	dimensionless
Alcohol partitioning parameters			
Parameter used to determine partition coefficient of IBA between aqueous and oleic pseudophases	AKWC7	4.671	dimensionless

Table B–1 Input Parameters for Simulation of a Surfactant/Polymer Coreflood Using UTCHEM

Parameter used to determine partition coefficient of IBA between aqueous and oleic pseudophases	AKWS7	1.79	dimensionless
Partition coefficient of monomeric IBA between surfactant and oleic pseudophases	AKM7	48.	dimensionless
Self-association constant of IBA in oleic pseudophase	AK7	35.31	dimensionless
Ratio of molar volume of IBA to equivalent molar volume of surfactant	PT7	0.222	dimensionless
Interfacial tension parameters			
Water-microemulsion interfacial tension parameters	G11	13.	dimensionless
	G12	-14.8	dimensionless
	G13	0.007	dimensionless
Oil-microemulsion interfacial tension parameters	G21	13.	dimensionless
	G22	-14.5	dimensionless
	G23	0.010	dimensionless
Log_{10} of oil/water interfacial tension	XIFTW	1.3	mN/m
Capillary—saturation curve parameters			
Capillary desaturation curve parameter for phase 1	T11	1865.	dimensionless
Capillary desaturation curve parameter for phase 2	T22	59074.	dimensionless
Capillary desaturation curve parameter for phase 3	T33	364.2	dimensionless
Residual saturation of phase 1 at high capillary no.	S1RC	0.0	fraction
Residual saturation of phase 2 at high capillary no.	S2RC	0.0	fraction
Residual saturation of phase 3 at high capillary no.	S3RC	0.0	fraction
Relative permeability parameters at low capillary no.			
Relative permeability endpoint of aqueous phase	P1RW	0.08	dimensionless
Relative permeability endpoint of oleic phase	P2RW	0.85	dimensionless
Relative permeability endpoint of microemulsion phase	P3RW	0.08	dimensionless
Relative permeability exponent of aqueous phase	E1W	2.7	dimensionless
Relative permeability exponent of oleic phase	E2W	1.6	dimensionless
Relative permeability exponent of microemulsion phase	E3W	2.7	dimensionless
Relative permeability parameters at high capillary no.			
Relative permeability endpoint of aqueous phase	P1RC	0.85	dimensionless
Relative permeability endpoint of oleic phase	P2RC	1.0	dimensionless
Relative permeability endpoint of microemulsion phase	P3RC	1.0	dimensionless
Relative permeability exponent of aqueous phase	E13C	1.5	dimensionless
Relative permeability exponent of oleic phase	E23C	1.6	dimensionless
Relative permeability exponent of microemulsion phase	E31C	0.5	dimensionless

Table B–1 Input Parameters for Simulation of a Surfactant/Polymer Coreflood Using UTCHEM

Phase viscosity parameters	ALPH1	4.0	dimensionless
	ALPH2	5.0	dimensionless
	ALPH3	-30.0	dimensionless
	ALPH4	0.9	dimensionless
	ALPH5	0.7	dimensionless
Zero-shear-rate viscosity parameters	AP1	52.0	$(wt\%)^{-1}$
	AP2	2430.0	$(wt\%)^{-2}$
	AP3	4,0000.0	$(wt\%)^{-3}$
Salinity effect parameters	BETAP	2.0	dimensionless
	CSE1	0.01	meq/ml
	SSLOPE	0.175	dimensionless
Shear-rate-dependent viscosity parameters	GAMMAC	4.0	$\frac{day(\mu m^2)^{1/2}}{m - sec}$
	GAMHF	20.0	sec^{-1}
	POWN	1.1	dimensionless